Published in final edited form as:

Nature. 2021 October ; 598(7881): 489–494. doi:10.1038/s41586-021-03952-y.

Hominini-Specific Regulation of *CBLN2* Increases Prefrontal Spinogenesis

Mikihito Shibata[1], **Kartik Pattabiraman**[1,2], **Sydney K. Muchnik**[1,3], **Navjot Kaur**[1], **Yury M Morozov**[1], **Xiaoyang Cheng**[4,5,6], **Stephen G. Waxman**[4,5,6], **Nenad Sestan**[1,2,3,7,8,9,10,*]

[1]Department of Neuroscience, Yale School of Medicine, New Haven, CT 06510, USA

[2]Yale Child Study Center, New Haven, CT 06510

[3]Department of Genetics, Yale School of Medicine, New Haven, CT 06510, USA

[4]Department of Neurology, Yale School of Medicine, New Haven, CT 06510, USA

[5]Center for Neuroscience and Regeneration Research, Yale University, New Haven, CT 06510, USA

[6]Rehabilitation Research Center, Veterans Affairs Connecticut Healthcare Center, West Haven, CT 06516, USA

[7]Department of Comparative Medicine, Yale School of Medicine, New Haven, CT 06510, USA

[8]Department of Psychiatry, Yale School of Medicine, New Haven, CT 06510, USA

[9]Program in Cellular Neuroscience, Neurodegeneration and Repair, New Haven, CT 06510, USA

[10]Kavli Institute for Neuroscience, Yale University, New Haven, CT 06520

Abstract

The similarities and differences between nervous systems of various species result from developmental constraints and specific adaptations [1–4]. Comparative analyses of the prefrontal cortex (PFC), a cerebral cortex region involved in higher-order cognition and complex social behaviors, have identified true and potential human-specific structural and molecular specializations [4–8], such as a PFC enriched anterior-posterior dendritic spine density gradient [5]. These changes are likely mediated by divergence in spatiotemporal gene regulation [9–17], which is particularly prominent in the midfetal human cortex [15,18–20]. Analyzing human and macaque transcriptomic data [15,20], we identified a transient PFC- and laminar-specific upregulation of cerebellin 2 (CBLN2), a neurexin (NRXN) and glutamate receptor delta GRID/GluD-associated synaptic organizer [21–27], during human midfetal development coinciding with the initiation

*Correspondence to Nenad Sestan (nenad.sestan@yale.edu).

Author Contributions

M.S., K.P., and N.S. designed research; M.S. and K.P. performed overall experiments, analyzed the data; S.K.M. analyzed RNA-seq, ChIP-seq and genomic sequence data; M.S. generated transgenic and knock-in mice; N.K. performed retrograde neuronal tracing with AAV, and analyzed the data. Y.M.M performed and analyzed electron microscopy experiments. X.C. and S.G.W. performed and analyzed preliminary electrophysiological analysis. N.S. conceived the study; M.S., K.P., and N.S. wrote the manuscript. All authors discussed the results and implications and commented on the manuscript at all stages.

Competing Financial Interests

The authors declare no competing financial interests.

of synaptogenesis. Moreover, we found that this difference in expression level and laminar distribution of *CBLN2* is due to Hominini-specific deletions containing SOX5 binding sites within a retinoic acid-responsive *CBLN2* enhancer. *In situ* genetic humanization of the mouse *Cbln2* enhancer drives increased and ectopic laminar *Cbln2* expression and promotes PFC dendritic spine formation. These findings suggest a genetic and molecular basis for the disproportionately increased dendritic spines in the Hominini PFC and a developmental mechanism linking dysfunction of the NRXN-GRID-CBLN2 complex to the pathogenesis of neuropsychiatric disorders.

Introduction

Expansion of the PFC in catarrhine primates is associated with increased dendritic complexity and synaptic spines of the pyramidal neurons compared to more posterior cortical association and sensory areas, creating an anterior-posterior gradient of synaptic density [28–30]. Moreover, this gradient is exaggerated in humans by the disproportionately high number of spines on pyramidal neurons in the human PFC as compared to the PFC of other analyzed primates [5]. Early neocortical synaptogenesis begins during the human midfetal period or equivalent developmental age in other mammals [31], proceeding in an anterior-posterior direction [32] and continues at an accelerated rate well beyond birth [33]. In our accompanying study [34], we identified a midfetal PFC-enriched gradient of retinoic acid (RA) concentration and pattern of gene expression in the human and macaque neocortex. Among the identified genes was synaptic organizer, *CBLN2*, which had the greatest loading of differentially expressed genes representing the anterior/frontal-posterior/temporal axis [35]. Members of the CBLN family encode secreted neuronal glycoproteins, which serve as excitatory and inhibitory synaptic organizing molecules [21–27]. Thus, we hypothesize that RA-mediated regulation of *CBLN2* expression in the developing PFC underlies the disproportionate number of synapses in the human PFC.

Cortical laminar divergence of prefrontal *CBLN2* expression

By analyzing RNA-seq data from eleven developing neocortical areas across human and macaque development from the BrainSpan and PsychENCODE projects [15,20], we identified a precocious and transient increase in human (1.9-fold change) and macaque (2.0-fold change) *CBLN2* expression in the major areas of the prospective PFC compared to the seven analyzed non-PFC areas during midfetal development (postconception weeks, PCW 13–24) or periods 4–6 according to Kang et al.[35] (Fig. 1a, Extended Data Fig. 1a,b). Around the time of late infancy, both human and macaque *CBLN2* expression levels are comparable across analyzed neocortical areas, despite modest but statistically significant increased expression in PFC areas compared to non-PFC areas (Human periods 7–10: 1.1-fold change; Macaque periods 7–10: 1.25-fold change Fig. 1a, Extended Data Fig. 1a), which continued at later adult ages (Humans periods 11–14: 1.1-fold change; Macaque periods 11–14: 1.2-fold change; Extended Data Fig. 1a,c). Analysis of the spatiotemporal expression profiles of the paralogs of *CBLN2* within each species revealed that *CBLN1* and *CBLN4* were significantly upregulated in human and macaque PFC, compared to non-PFC areas (Extended Data Fig. 2). While none of the binding partners of the CBLN family

members, *NRXN1,2,3* and *GRID1,2,* showed distinct PFC upregulation during midfetal development, all were expressed in the PFC with increasing expression levels during development (Extended Data Fig. 2c).

Previous bulk tissue transcriptomic studies have also reported an anterior-posterior gradient of *CBLN2* expression in the human midfetal neocortex [18,36,37]. We confirmed this finding using *in situ* hybridization (PCW 21 and 22) and single cell RNA-seq data, showing that *CBLN2* was detected broadly in neurons of prospective upper layers (L) 2 to 4 and deeper L5 and 6 of the PFC, but faintly posteriorly (Fig. 1b; Extended Data Fig. 1b,d). We also identified an anterior-posterior gradient of *Cbln2* expression in macaque (postconception day, PCD 110, and 140) and mouse (Postnatal day, PD 0) at equivalent developmental ages (Fig. 1b, Extended Fig. 1b, 3a,b). Interestingly, in macaque, *Cbln2* expression was mostly observed in L2 corresponding to the prospective upper layers with noticeably weaker expression in the deeper layers (Fig. 1b). In mice, *Cbln2* was mostly restricted to the prospective upper layers (Fig. 1b, Extended Data Fig. 3b). Together, our analysis found a progressive extension of *CBLN2* expression into the deeper layers of the midfetal PFC in humans compared to macaques, and in macaques compared to mice.

Hominini-specific deletions in RA-responsive *CBLN2* enhancer

In order to understand regulatory mechanisms of *CBLN2* expression in the midfetal PFC, we analyzed publicly available datasets on the regulatory landscape of developing mouse and human brains generated by the ENCODE and PsychENCODE projects [20,38]. Around the mouse *Cbln2* locus, we identified three putative *cis*-regulatory elements marked as DNase 1 hypersensitive sites, which we designated as *Cbln2* enhancer 1 (*Cbln2* E1, 1452 bp), enhancer 2 (*Cbln2* E2, 1005 bp), and promoter (*Cbln2* Pro, 316 bp; Fig. 1c, **top**). The sequences of these putative *cis*-regulatory elements are moderately conserved between mouse and human (E1, 76.3%; E2, 84.3%; and Pro, 70.0%). Of note, mouse *Cbln2* E2 showed DNase 1 hypersensitivity peaks only in PCD 14.5 samples and *Cbln2* E1 only in 8 postnatal weeks (PW) samples (Fig. 1c, **top**). Analysis of genomic sites with differential distribution of H3K27ac, a mark of active enhancers, in the developing and adult human dorsolateral PFC (dlPFC/DFC) indicates that *CBLN2* Pro is active at all three analyzed time points (midfetal, early infancy and adult ages), while *CBLN2* E1 is active during midfetal age and infancy, and *CBLN2* E2 is only active during midfetal age (Fig 1c, **bottom**).

We next assessed the activity of these putative regulatory regions using transgenic mouse lines in which a *lacZ* expression cassette was placed downstream of mouse *Cbln2* E1, *Cbln2* E2, or *Cbln2* Pro. While *Cbln2* E1-*lacZ* and *Cbln2* Pro-*lacZ* transgenic lines exhibited no detectable *lacZ* expression (0 of 10 founders) in the developing cortex between PCD 17 and 18, 50% of *Cbln2* E2-*lacZ* transgenics (3 of 6 founders) showed *lacZ* expression, with two of three independent lines recapitulating endogenous frontal cortex-enriched *Cbln2* expression (Fig. 1d; Extended Data Fig. 3c). These findings indicate that *Cbln2* E2 is an enhancer that drives expression in the mouse neonatal frontal cortex.

Given the presence of *CBLN2* E2 in human, macaque and mouse, we hypothesized that sequence differences between the orthologs may underlie the species-specific expression

pattern of *CBLN2*. Comparative genomic and phylogenetic analysis identified two separate deletions (122 bp, 20 bp) and insertion (84 bp) in the sequence of the human *CBLN2* E2 ortholog as compared to the sequence of the mouse *Cbln2* E2 (Fig. 2a). Further comparison across multiple vertebrates revealed that two of the three deleted sequences are jointly absent only in extant members of the Hominini clade (human, common chimpanzee, and bonobo) (Extended Data Fig. 4a,c, 5). The first two of these sequences, which we named Hominini-specific deletion 1 and 2 (HSD1 and 2, Fig. 2a), are highly conserved among other analyzed Haplorhini (gorilla, macaque), Strepsirrhini (lemur), and mouse (Fig. 2a, Extended Data Fig. 4a,c 5). The third inserted sequence (I3) sequence was detected only in mouse and rat of the Muroidea species analyzed (Extended Data Fig. 4a, 5). Interestingly, we did not detect genomic regions orthologous to *Cbln2* E2 in analyzed non-placental mammals and non-mammalian chordates, although they do possess the *Cbln2* gene (Extended Data Fig. 5).

In our accompanying study [34], we found that RA receptors *RXRG* and *RARB* are upregulated in the midfetal frontal lobe and that *Cbln2* expression was reduced in neonatal *Rxrg* and *Rarb* double knockout mice. Thus, we screened for and identified multiple putative RAR-RXR tandem binding sites in *CBLN2* E2 (Fig 2a, Extended Data Fig. 4a). Consistent with these findings, we found that overexpression of RXRG and RARB in Neuro2a cell line activated human, chimpanzee, gorilla, macaque, and mouse orthologs of *CBLN2* E2 in *in vitro* luciferase reporter assays more than overexpression of either individually (Fig. 2b; Extended Data Fig. 6a), consistent with previous reports showing that RA receptors exert their effects as heterodimers [39,40].

Hominini-specific repression of *CBLN2* E2 enhancer by SOX5

In addition to RA receptors, analysis of *Cbln2* E2 also identified multiple conserved putative SOX5 binding sites, including three in HSD1 and a fourth in HSD2 (Fig. 2a, Extended Data Fig. 4a,b), as well as non-conserved sites in mouse HSD1 and 2 orthologs, and in I3 (Fig. 2a). Screening for gained putative human and hominini-specific transcription factor (TF) binding sites identified only a few generic TF binding sites (Extended Data Table 1). Thus, we focused on putative SOX5 binding sites given their loss in Hominini E2 and the role of SOX5 in the specification and development of deep layers cortical projection neurons[41,42]. We found that mouse *Cbln2* E2 activation by RXRG-RARB heterodimer was suppressed by SOX5 in a dose-dependent manner, whereas human and chimpanzee *CBLN2* E2 showed no significant suppression by SOX5 at the same doses (Fig. 2b; Extended Data Fig. 6a). Differential suppression of *Cbln2* E2 activation was not a consequence of sequence differences between mouse and human SOX5, as activation of mouse *Cbln2* E2 was suppressed by both mouse and human SOX5 (Fig. 2b; Extended Data Fig. 6b). Activation of macaque and gorilla *Cbln2* E2 showed intermediate suppression of activity at the same doses of SOX5 (Fig. 2b; Extended Data Fig. 6a). Deletion of HSD1, HSD2, and I3 in mouse, or HSD1 and HSD2 in macaque, abolished suppression by SOX5, suggesting that these regions mediate SOX5 suppression (Fig. 2b). Testing for direct *in vivo* binding using chromatin immunoprecipitation followed by PCR (ChIP-PCR) assays found that endogenous SOX5 bound *Cbln2* E2 but not *Cbln2* E1 (Fig. 2c).

To understand the functional significance of SOX5 repression of *Cbln2* E2 *in vivo*, we examined *Cbln2* cortical expression by creating a cortex-specific *Sox5* conditional knockout (cKO; *Sox5* loxP/loxP; *Emx1-Cre*) mouse. As predicted by luciferase assays, the absence of SOX5 led to ectopic expression of *Cbln2* in deeper layers of the neonatal frontal cortex (Fig. 2d,e, Extended Data Fig. 6c). There was also an increase and posterior extension of *Cbln2* expression in the upper layers (Fig. 2d,e, Extended Data Fig. 6c), likely due to previously described transient *Sox5* expression in these layers[41]. Consistent with these results, the 5' segment of *Cbln2* E2 lacking the two HSD sequences and I3 (*Cbln2* E2-Fr1) was not suppressed by SOX5 in luciferase assay (Extended Data Fig. 6d,f). Furthermore, a transgenic mouse line expressing *lacZ* under the transcriptional control of *Cbln2* E2-Fr1, showed deep layer expression of *lacZ* as compared to *Cbln2* E2 (Extended Data Fig. 6d,e). Taken together, these observations suggest SOX5 directly represses *Cbln2* expression in the deep layers of a neonatal mouse and midfetal macaque (and likely other non-Hominin primates) frontal cortex by binding HSD sites in *Cbln2* E2.

Humanized *Cbln2* E2 increases spinogenesis in mouse PFC

To test whether human *CBLN2* E2 is sufficient to drive a human-like pattern of *Cbln2* expression in the mouse neonatal frontal cortex, we generated a knock-in mouse in which the *Cbln2* E2 was replaced *in situ* (in the orthologous position) with the corresponding human *CBLN2* E2 using the CRISPR-Cas9 genome editing technique (Extended Data Fig. 7a–c). The engineered mice carrying homozygous humanized *Cbln2* E2 (h*Cbln2* E2) in both alleles (*Homo sapiens*;*Homo sapiens*, *Hs;Hs*) were viable and fertile, and the expression of the cortical upper layer specific marker, *Cux2*, and SOX5 were comparable to homozygous wildtype (WT) *Cbln2* E2 (*Mus musculus;Mus musculus*, *Mm;Mm*) mice (Fig. 3c), indicating that genetically humanized h*Cbln2* E2 grossly functions as the mouse ortholog. Neocortical *Cbln2* expression at PD 0 was increased by 21.7% in h*Cbln2* E2 (*Hs;Hs*), as compared to WT by quantitative RT-PCR (Extended Data Fig. 7d). Analysis of expression by *in situ* hybridization showed that *Cbln2* was also transiently upregulated in both prospective upper and deeper layers of the h*Cbln2* E2 PFC at PCD 18 and PD 1, but not at PCD 16 (Fig. 3a,b; Extended Data Fig. 8). After PD 1, *Cbln2* expression extended into the deeper layers of PFC, coinciding with the down-regulation of SOX5 protein expression (Extended Data Fig. 9) in both h*Cbln2* E2 and WT *Cbln2* E2.

Members of the CBLN family have been reported to regulate synapse development and function [21–27]. Therefore, we hypothesized that a transient increase in *Cbln2* expression in the h*Cbln2* E2 PFC will lead to increased postsynaptic structures and synapse number. We quantified both excitatory and inhibitory postsynaptic density in the medial PFC (mPFC), primary somatosensory area (SSp), and primary visual (VISp) area using immunostaining for postsynaptic proteins PSD-95/DLG4 and gephyrin (GPHN), respectively. In h*Cbln2* E2 (*Hs;Hs*) mice, we observed an increase in the density of PSD-95-immunopositive excitatory postsynaptic puncta in both upper (39.5%) and deep layers (47.9%) in the mPFC but not in the SSp and VISp, where *Cbln2* expression is not altered, at PD 0 (Extended Data Fig. 10a,b). A similar increase in PSD-95-immunopositive puncta in the mPFC was identified in the *Sox5* conditional KO mice (58% for upper layers, 40% for deep layers; Extended Data Fig. 10b). We also observed an increase in the density of GPHN-immunopositive

inhibitory postsynaptic puncta number in both upper (24.2%) and deep layers (37.9%) at PD 0 in the h*Cbln2* E2 PFC but not in the SSp and VISp cortex (Extended Data Fig. 10c,d). In the *Sox5* conditional KO mice, anti-GPHN immunostaining revealed a similar increase in the density of inhibitory postsynaptic puncta (27.3% for upper layers, 39.4% for deep layers; Extended Data Fig. 10d). At PD 60, an increase in the density of PSD-95-immunopositive postsynaptic puncta was observed in deep layers of humanized *CBLN2* E2 mice (21.4%), and no significant changes were observed in the density of GPHN-immunopositive postsynaptic puncta (Extended Data Fig. 10b,d).

We confirmed the PFC-specific increase in excitatory postsynaptic structures in the h*Cbln2* E2 (*Hs;Hs*) mice by quantifying dendritic spines using two different strategies. Using Golgi staining, we identified an increase in mature mushroom shaped spines and long thin spines in both the upper and deep layers of h*Cbln2* E2 (*Hs;Hs*) mPFC (Extended Data Fig. 11a) but not in the SSP or VISp (Extended Data Fig. 11b,c). Similarly, we identified an increase in dendritic spines in apical and basal dendrites of both retrogradely labelled upper layer callosally projecting neurons and L5B subcerebrally projecting neurons of the h*Cbln2* E2 (*Hs;Hs*) mPFC compared to WT littermates (Fig. 4a,c). To assess whether dendritic spines in the WT and h*Cbln2* E2 (*Hs;Hs*) mPFC form synapses, we conducted 3D reconstruction from serial section electron microscopy at PD 60. We found 91.4% of dendritic spines in the h*Cbln2* E2 mPFC had presynaptic innervation, similar to *Cbln2* E2 control (Extended Fig. 11f,g), thus providing evidence against an increase in non-synaptic dendritic spines in h*Cbln2* E2 (*Hs;Hs*). Furthermore, we also identified a significant increase overlapping PSD-95/DLG4-immunolabelled postsynaptic and synaptophysin (SYP)-immunolabelled presynaptic puncta in both upper (15.4%) and deep layer (38.6%) of the early postnatal h*Cbln2* E2 (*Hs;Hs*) mPFC (Extended Fig. 11d,e). Finally, as increase in dendritic spines and synapse number could be secondary to increased dendritic complexity, which has also been described in human PFC [5], we compared the dendritic arbors in WT *Cbln2* E2 compared to h*Cbln2* E2. We found no significant difference in dendritic complexity in Golgi and retrograde viral tracers labelled dendrites arbors by Sholl Analysis in PFC, SSp or VISp (Fig. 4b; Extended Data Fig. 11a–c).

Discussion

In this study, we describe a potential CBLN2-based molecular mechanism and underlying genetic basis for the anterior-posterior gradient of neocortical synaptogenesis and disproportionate increase in dendritic spines within the human PFC. In our accompanying paper [34], we identified that loss of RA signaling in the developing mouse mPFC leads to both reduced expression of *Cbln2* and reduced density of excitatory dendritic spines. Regulation of *Cbln2* E2 by RXRG and RARB, provides a direct link between these two finding, and may be part of a more complex gene regulatory network regulating development and adaptive changes in PFC connectivity. Furthermore, species-specific regulation of *CBLN2* expression is likely only one aspect of phylogenetic differences in connectivity, including described inter-hominin differences [5,6] and accelerated expression of synaptic genes in the developing human neocortex, compared to macaque [15].

While CBLN2 has been implicated in OCD, SCZ, and Tourette's syndrome [43], it serves as ligands for multiple NRXNs and GRID1, which are ASD- and SCZ-associated proteins, respectively [44,45]. Multiple lines of evidence have shown that ASD and SCZ risk genes, converge in time, brain region, cell type and cell compartment with strong evidence for convergence in synapses as well as glutamatergic projection neurons and frontal cortex during human midfetal development [46,47]. Consistent with these findings, alterations in the levels of some synaptic proteins and connectivity within the frontal lobe have been described as the possible underlying pathophysiology of both ASD and SCZ [44,48,] with dysfunction in the NXRN-GRID trans-synaptic complex, which includes CBLNs, being a putative mechanism and target for interventions.

Methods

Analysis of human and macaque transcriptomic data

Developing human and macaque brain RNA-seq data (counts file) with its metadata information was obtained from BrainSpan (brainspan.org) and PsychENCODE (development.psychencode.org, evolution.psychencode.org) projects [15,20]. Timeline of human and macaque development and associated periods were designed by Kang et al. [35]. Predicted ages for macaque samples were calculated via the *TranscriptomeAge* algorithm described in Zhu et al. [15]. To perform statistical comparisons, samples from various developmental periods were grouped (periods 4–6, 7–10, and 11–14) and a two-tailed Student's t-test was used to compare gene expression levels between brain regions and species.

Animals

All experiments using animals were performed in accordance with protocols approved by the Yale University Institutional Animal Care and Use Committee (IACUC). All studies using mice (*Mus musculus*) and rhesus macaques (*Macaca mulatta*) were performed in accordance with protocols approved by Yale University's Institutional Animal Care and Use Committee and NIH guidelines. The animals were housed, and timed-pregnant prenatal and postnatal mouse and monkey brains were obtained in-house at the Yale Animal Resource Center. Mice were reared in group housing less than five mice per cage at 25 °C and 56% humidity in a 12h light:12h dark cycle and provided food and water ad libitum with veterinary care provided by Yale Animal Resource Center. Animals were maintained on the C57BL/6J background. Both sexes were used and randomly assigned for all experiments. The day on which a vaginal plug was observed in mice was designated as PCD 0.5. Mice carrying the floxed *Sox5* allele were a kind gift from Véronique Lefebvre [49].

Plasmid construction

For construction of expression vectors used for luciferase assays, full-length cDNAs (Human *SOX5*, clone ID 30343519; mouse *Rarb*, clone ID 30608242; mouse *Rxrg*, clone ID 5707723; all purchased from GE Healthcare) were inserted into pCAGIG vector (Addgene plasmid #11159). For luciferase reporter plasmids, human, chimpanzee, gorilla, macaque, and mouse *Cbln2* E2 fragments were PCR-amplified from genomic DNA of individual

species and inserted into pGL4.24 vector (Promega, Cat. E8421). The sequences of the PCR primers and synthetic oligonucleotides are listed in Extended Data Table 2.

Postmortem human and macaque tissue

This study was conducted using postmortem human brain specimens or RNA-seq data generated previously [20] from tissue collections at the Department of Neuroscience at Yale School of Medicine, the Brain and Tissue Bank for Developmental Disorders at the University of Maryland, the Clinical Brain Disorders Branch of the National Institute of Mental Health, the Human Fetal Tissue Repository at the Albert Einstein College of Medicine, the Birth Defects Research Laboratory at the University of Washington (R24HD000836), Advanced Bioscience Resources and the Joint MRC–Wellcome Trust Human Developmental Biology Resource (www.hdbr.org; MR/R006237/1). Tissue was collected after obtaining parental or next of kin consent and with approval by the institutional review boards at each institution from which tissue specimens were obtained, the Yale University and the National Institutes of Health. Donated deidentified tissue was handled in accordance with ethical guidelines and regulations for the research use of human brain tissue set forth by the National Institutes of Health (https://oir.nih.gov/sites/default/files/uploads/sourcebook/documents/ethical_conduct/guidelines-biospecimen.pdf) and the WMA Declaration of Helsinki (https://www.wma.net/policies-post/wma-declaration-of-helsinki-ethical-principles-for-medical-research-involving-human-subjects/). All available non-identifying information was recorded for each specimen. No obvious signs of neuropathological alterations were observed in any of the human, macaque or mouse specimens analyzed in this study. The postmortem interval was defined as hours between time of death and time when tissue samples were fresh frozen or started to undergo fixation process.

Transcription factor binding site (TFBS) analysis

The software FIMO from the MEME suite (ver. 4.12.0) was used to identify putative transcription factor binding sites in the human sequence of the *CBLN2* E2 enhancer. For this analysis, a set of transcription factor motifs from the JASPAR 2018 dataset (http://jaspar2018.genereg.net/) [50] were used. Then, MAF (Multiple Alignment Format) files were downloaded from the multiz100way table of the UCSC genome browser. An in-house script was used to extract the sequence of each TFBS in each species from the MAF file and identify mutations in core positions of the motif. TFBS were considered conserved in a particular species if they had no mutations in core positions and were considered present in a clade if the TFBS was conserved in at least 25% of the species in the clade. To check for potential loss of TFBS regulatory mechanisms due to the deletions HSD1, HSD2, and I3, we looked for TFBS that are found in these regions and conserved in multiple species that do not have the deletions. To do so, the software FIMO was used to identify instances of transcription factor binding motifs from the JASPAR database. This was performed in two species for each deletion (mouse and macaque for HSD1 and 2, and mouse and rat for I3). Then, the coordinates of putative TFBSs in the regions of interest in macaque and rat were translated to mm10 coordinates using LiftOver (downloaded on May 3rd, 2017) and manually compared to the TFBS identified in the mouse sequence. Instances of the same transcription factor binding motif at the same location in both datasets were considered

putatively conserved. SOX5-binding sites and RA receptors binding sites of mouse and human were identified using JASPAR2018 [51]. The binding sites from other animal species were identified by conservation. RA receptors binding sites include those of RARA::RXRA, RARA::RXRG, RARA, RARB, RARG, RXRA, RXRB, and RXRG.

Generation of transgenic reporter mice

Cbln2 E2 and its related fragments were PCR-amplified from mouse genomic DNA and ligated into pBgn-*lacZ* [52]. Vector was linearized with BglII and KpnI and purified by gel separation followed by phenol/chloroform extraction. Transgene fragment was diluted into microinjection buffer (5 mM Tris-HCl, 0.1 mM EDTA), and injected into the pronucleus of fertilized eggs from B6SJLF1/J mouse purchased from The Jackson Laboratory. Transgenic mice were screened for the presence of transgenes by PCR using the *lacZ* primer set listed in Extended Data Table 2.

Generation of humanized *Cbln2* E2 knock-in mice

The overall strategy for the generation of humanized *Cbln2* E2 (h*Cbln2* E2) follows a previously described protocol [53]. The targeting vector carrying h*Cbln2* E2 mouse was constructed as follows: mouse genomic DNA fragments of 1601 bp (chr18: 86721709–86723309, GRCm38/mm10) and 1909 bp (chr18: 86724521–86726429, GRCm38/mm10) flanking the region containing *Cbln2* E2 (chr18: 86723310–86724520, GRCm38/mm10) were PCR-amplified as left and right arm, respectively, using mouse genomic DNA as template. An 852 bp fragment containing human *CBLN2* E2 (chr18: 72530473–72531324, GRCh38/hg38) was PCR-amplified using human genomic DNA as a template. These three DNA fragments were ligated into *XhoI*, *HindIII* and *ClaI* sites of the PL451 vector [54]. For the construction of the templates of guidance RNA, two sets of top and bottom strand oligomers (see Extended Data Table 2) directing the double strand break at mouse left and right arm were annealed and ligated into *BbsI* site of pX330-U6-Chimeric_BB-CBh-hSpCas9 vector [55], which was purchased from Addgene (Plasmid #42230). After amplification of insert with T7-tagged primers (see Extended Data Table 2), guidance RNAs were synthesized by T7 RNA polymerase. The coding region of Cas9 was PCR-amplified using pX330-U6-Chimeric_BB-CBh-hSpCas9 as a template and inserted into the pSP64 Poly(A) vector (Promega, Cat. 1241). Vector were digested and linearized with *EcoRI*. Cas9 mRNA was synthesized by SP6 RNA polymerase. Guidance RNAs and Cas9 mRNA were purified by MEGAclear Transcription Clean-Up Kit (Ambion, Cat. AM1908). The targeting vector, Cas9 mRNA, and two guidance RNAs were mixed at a concentration of (10 ng; 100 ng; 100 ng; 200 ng μl^{-1}) in the microinjection buffer (5mM Tris-HCl pH7.5; 0.1M EDTA) and injected into the pronuclei of fertilized eggs from the B6SJLF1/J mouse strain. Which was purchased from The Jackson Laboratory. The fertilized eggs were then transferred to uterus of female CD-1, purchased from Charles River Laboratories. The first generation (F0) mice with recombined allele were identified by long-distance PCR with a primer set (mP3/mP4) designed outside of targeting vector (Extended Data Table 2, Extended Data Fig. 7a), and confirmed by sequencing. The germ line transmission in F1 generation was confirmed by nested PCR using the primer set of mP3/mP4, followed by hP1/P2 (Extended Data Fig. 7b,c), to exclude the possibility of detecting targeting vector randomly integrated into the

genomic DNA. Mice in the following generation were genotyped by PCR with mP1/mP2 and hP1/P2 as indicated in Extended Data Fig. 7.

In situ hybridization

Whole-mount and section *in situ* hybridization were performed as described previously [56]. Antisense digoxigenin (DIG)-labeled RNA probes were synthesized using DIG or Fluorescein RNA Labeling Mix (Roche, Cat. 11277073910). Human and mouse *Cbln2* cDNA, and mouse *Cux2* cDNA were obtained from GE Healthcare (Clone ID 5727802, 6412317, and 30532644, respectively). Macaque *Cbln2* cDNA was synthesized using total RNA from adult macaque dlPFC/DFC region. The PCR fragment was ligated into pCRII vector (ThermoFisher Scientific, Cat. K206001). Tissue sections were obtained from PCW 21 and 22 de-identified postmortem human brains, PCD 110 and 140 postmortem macaque brains, and mouse postmortem brains of various developmental ages. *In situ* hybridization experiments were repeated using these two sets. Images were taken using Aperio CS2 HR Scanner (Leica; Wetzlar, Germany) and processed by Aperio ImageScope 12.4.3.5008 (Leica).

Immunohistochemistry

Postmortem brains were dissected and fixed with 4% paraformaldehyde overnight at 4°C, followed by 30% sucrose/PBS and embedding in O.C.T. Compound (ThermoFisher Scientific, Cat. 23-730-572). Brains were sectioned at 15–20 μm by cryostat (Leica CM3050S) after they were frozen. For antigen retrieval, sections were treated with R-Buffer AG pH 6.0 (Electron Microscopy Sciences, Cat. 62707–10) for 20 min at 120 °C. The density of excitatory and inhibitory postsynaptic puncta was quantified using immunostaining of PSD-95 (also known as DLG4) [57] and gephyrin (GPHN) [58], respectively. The sources of primary antibodies were anti-PSD-95/DLG4 (1:500; Invitrogen, Cat. 51–6900), anti-GPHN (1:500; Synaptic Systems, Cat. 147011), anti-SYP (1:2000, Sigma-Aldrich, Cat. SAB4200544), anti-SOX5 (1:500; Abcam, Cat. ab94396), and anti-BCL11B/CTIP2 (1:500, Abcam, Cat. ab18465). Secondary antibodies: Alexa Fluor 488-, or 594- conjugated AffiniPure Donkey anti-Rabbit IgG (Jackson ImmunoResearch). For all microscopic analysis, LSM META (Zeiss), and LSM software ZEN2009 were used.

Quantification of postsynaptic and presynaptic puncta marked by immunostaining

For each cortical area, using both the 488 nm channel to detect PSD-95 (also known as DLG4) or gephyrin (GPHN) and the 594 nm channel to detect BCL11B or synaptophysin (SYP), seven serial optical sections at 0.8 μm intervals over a total depth of 5 μm were imaged and the 2nd, 4th, and 6th images were eliminated from further analysis to avoid overlap in counting [59]. Area of each image is 0.079 mm^2. The number of PSD-95, SYP-, or GPHN-immunopositive puncta on each image was counted using ImageJ (ver.2.0.0-rc-69/1.52p) using the automated Analyze Particles function using a threshold of 985 to 4095, determined based on multiple WT *Cbln2* E2 and humanized hCbln2 E2 images. BCL11B-immunonegative cells were considered as L2-4, and BCL11B-immunopositive nuclei were considered as L 5. At least three sections from each animal were selected for counting, and at least 3 animals for each genotype were used.

Golgi staining

A FD Rapid GolgiStain Kit (FD NeuroTechnologies, Cat. PK401) was used to compare neuronal morphologies (~5 basal dendrites/neuron; ~4 neurons per mouse) throughout the prefrontal cortex, S1C, and V1C of WT *Cbln2* E2 (N = 3) and humanized *hCbln2* E2 (N = 3) mice aged P60. The manufacturer's protocol was followed, incubating brains in solution A+B for 21 days and solution C for 7 days before sectioning and mounting on TOMO adhesion microscope slides (Matsunami, Cat. TOM-11). The sections were dried overnight, washed and developed by immersing the slides in solution D and solution E mixed in equal amounts for 10 min. The slides were washed twice with distilled water and dehydrated in grades of ethanol and xylene. After cover-slipped with Permount (Fisher Scientific, Cat. 15820100), sections were imaged on a Nikon SDC microscope enabled with brightfield.

Retrograde neuronal tracing with adeno-associated viruses

To differentiate between the callosally and subcerebrally projecting neurons in the mPFC, we performed dual retrograde injections into the contralateral mPFC and the ipsilateral basal pontine nuclei, respectively at PD 30. Briefly, animals were anesthetized by injecting Ketamine/Xylazine solution and head fixed in the stereotactic frame. Thirty minutes prior to surgery, buprenorphine was administered. After lubricating the eyes and shaving the fur, and incision of < 1mm was made. A craniotomy was made with the round 0.5 mm drill bit at the desired co-ordinates (for mPFC: ML ±0.35, AP 1.5, DV 2.5 and for contralateral Pons: ML ± 0.5, AP −4.0 and DV 5.5 from bregma). Using a Hamilton neuros syringe (0.5 ml), we injected 50 nl of *AAVrg-Cag-Tdt* (Addgene, 59462-AAVrg) into the mPFC and 150 nl of *AAVrg-Cag-Gfp* (Addgene, 37825-AAVrg) into the pons at P30. To prevent the virus from spreading along the injection tract, the needle was held in place for at least 10 min. After injections, the skin was sutured and animals were returned to the cage. Approximately 3 weeks later (PD 60), the animals were sacrificed and brains were collected. The brains were coronally sectioned on vibratome to obtain 70 μm thick sections. After staining the sections with anti-GFP antibody (1:500, Abcam, Cat. ab13970) and anti-RFP antibodies (1:500, Abcam, Cat. ab124754), the sections were imaged in LSM 800 microscope (ZEISS).

Quantification of dendritic spines and dendritic arbor

The images of entire neurons were acquired at 20X magnification. Nearly 44–50 images/Z stack were obtained to cover the entire thickness of dendrites. For spine counts, the z stack images were opened in the Reconstruct 1.1.0.0. (Boston, MA, USA) publicly available at http://www.bu.edu/neural/Reconstruct.html [60] and a new series was recreated which enabled us to move across different stacks across z-planes in same image. Whole dendrite was subdivided into segments of 10 μm and number of spines across whole thickness were traced for length and breadth of each spine. Length and breadth ratio was used to determine the spine subtype as described earlier [61,62]. After the analysis for each class of spine, standard deviation and p-values are calculated using two-way Anova with Sidak's multiple comparison method. For Sholl analysis, z-stack images were opened in ImageJ (ver. 2.0.0-rc-69/1.52p) and dendritic arbors were manually traced using the NeuronJ plugin [63]. Dendritic complexity was then quantified and plotted using the Sholl Analysis option.

Processing, analysis, and image visualization

For select figure images, slides background was removed and pseudocolored white for improved clarity, as in Fig 1b. To allow robust visualization and analysis, images depicting immunohistochemistry using antibody against PSD-95/DGL4 and GPHN have been inverted and/or pseudocolored, as in Fig. 4.

ChIP-sequencing data analysis

H3K27ac ChIP-seq from the developing human brain was obtained and peaks were called by Li et al. [20] that were converted to the mm10 genome build using LiftOver [64] and visualized using the Integrative Genomics Viewer [65]. DNase 1 hypersensitivity annotation was obtained and visualized via the UCSC Genome Browser [66,67].

Luciferase assays

Neuro-2a cells were transfected using Lipofectamine 2000 (ThermoFisher Scientific, Cat. 11668019) with either mouse or human pCAGIG-*Sox5*, *Rxrg*, *Rarb*, or empty pCAGIG, together with one of the pGL4.24 luciferase vectors generated with enhancer sequences as described above. pGL4.73 *Renilla* luciferase plasmid (Promega, Cat. E6911) was co-transfected to control for transfection efficiency. The luciferase assays were performed 48 h after transfection using the Dual-Luciferase Reporter Assay System (Promega, Cat. E1910) according to the manufacturer's instructions. Luciferase activity were measured and quantified by GloMax®-Multi Detection System (Promega).

Chromatin immunoprecipitation (ChIP)

The anterior half of cortices from PD 0 mice were dissociated then cross-linked with 1% formaldehyde and processed using EZ-ChIP kit (Sigma-Aldrich, Cat. 17–371). Chromatin fragments bound by endogenous mouse SOX5 were pulled down by anti-SOX5 (Abcam, Cat. ab94396), anti-POL2 antibody (1:1000, Millipore-Sigma, Cat. 05–623, included in the kit), or random IgG control (included in the kit), then detected by PCR using E2-ChIP-F and E2-ChIP-R or E1-ChIP-F, and E1-ChIP-R primers (see Extended Data Table 2).

Quantitative reverse transcription-PCR

Total RNA was isolated using Trizol (Thermo-Fisher Scientific, Cat. 15596026) from freshly dissected neocortices after removal of the olfactory bulb, hippocampus, and striatum. cDNAs were prepared using SuperScript II (Thermo-Fisher Scientific, Cat. 18064022) from more than three independent WT littermates and humanized *hCbln2* E2 brains. Quantitative reverse transcription-PCR was performed as described previously [68] using 7000HT Sequence Detection System (Applied Biosystems). At least three biological replicates per transcript were used for every reaction. The copy number of transcripts was normalized against the house keeping TATA-binding protein (TBP) transcript level. For *Cbln2* and *Tbp* primer sets, correlation (R2) was higher than 0.98, and the slope was −3.1 to −3.6 in each standard curve. Primers were designed in a single exon and are listed in Extended Data Table 2.

3D reconstruction of dendrites and denritic spines using electron microscopy

PD 60 WT *Cbln2* E2 and humanized h*Cbln2* E2 mice (N = 3 for each genotype) were intracardially perfused with fixative containing 4% paraformaldehyde and 1% glutaraldehyde in 0.1 M phosphate buffer (pH 7.4). Brains were removed and immersed in same fixative for 3–4 days at 4°C. Coronal 60-mm-thick slices through prefrontal cortex were cut with a vibrotom, post-fixed with 1% OsO_4, dehydrated in ethanol, embedded in epoxy resin Durcupan (ACM; Fluka, Buchs, Switzerland) and polymerized on microscope slides. Ultrathin sectioning and electron microscopic investigation were performed as we previously described [69,70] with minor modifications as follow. Segments of the mPFC were dissected and re-embedded into Durcupan blocks. Serial 60-nm-thick sections from mPFC L2-3 were cut by Leica UC7 ultramicrotome, collected on one-slot grids covered with Butvar B-98 films (EMS, Hatfield, PA, USA) and stained with lead citrate. Series of 48–51 consecutive images were photographed with Talos L120C electron microscope (ThermoFisher Scientific, Boston, MA, USA) at 5300 X magnification. For serial imaging, random neuropil segments were chosen although avoiding cell bodies and blood capillaries. 3D reconstructions were performed using the computer program Reconstruct 1.1.0.0. (Boston, MA, USA) publicly available at http://www.bu.edu/neural/Reconstruct.html [60]. Sixteen -representable dendrite fragments were traced in the serial images and their innervated spines and non-innervated spine-like membrane protrusions were counted. Percentage of innervated spines among all the protrusions were calculated for each animal.

Reporting summary

Further information on research design is available in the Nature Research Reporting Summary linked to this paper.

Data availability

None

Extended Data

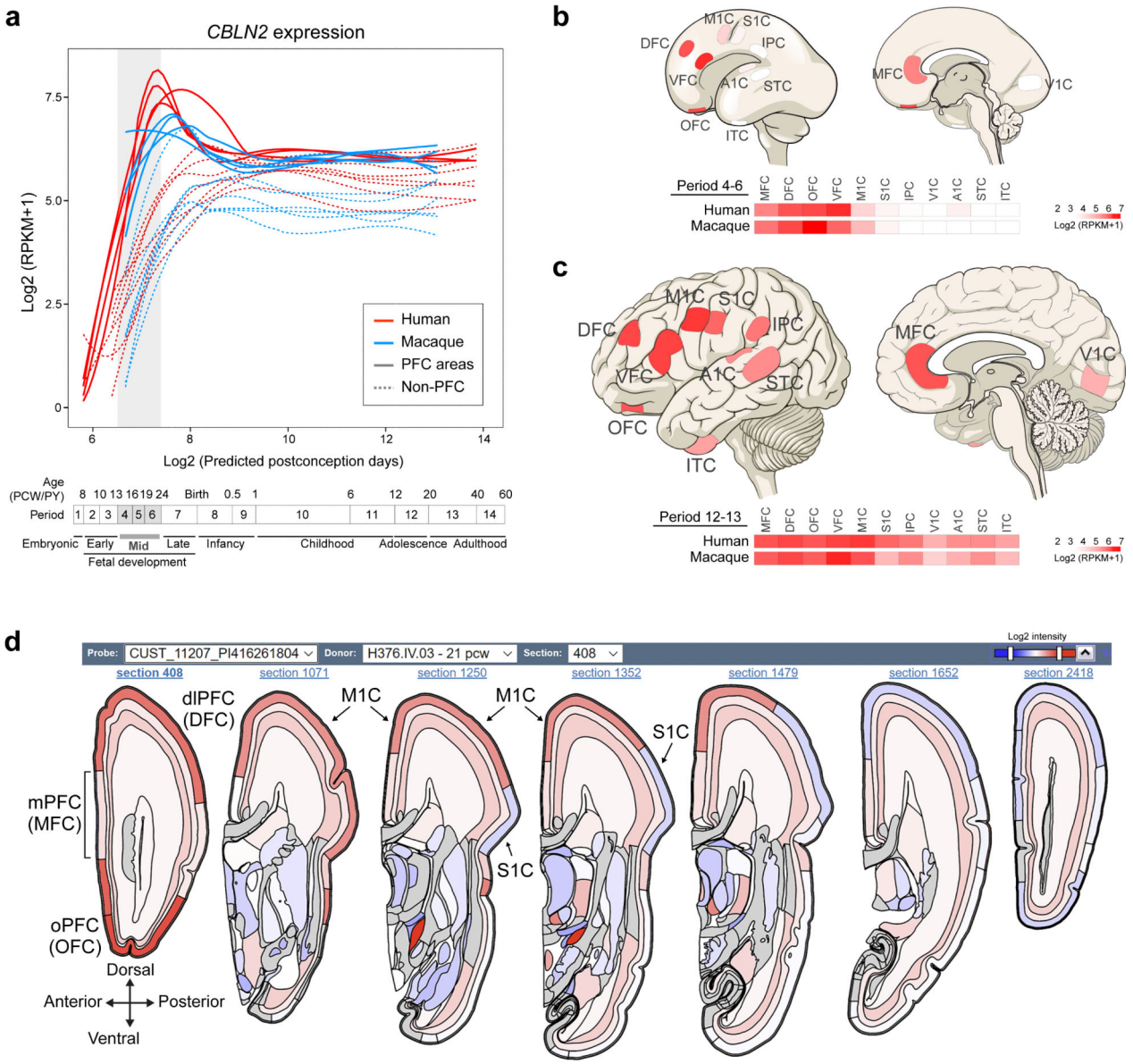

Extended Data Fig. 1 |. Spatiotemporal expression of *CBLN2* in the human and macaque neocortex.

a-c, Spatiotemporal expression of *CBLN2* expression in the human and macaque cerebral cortex during development base on BrainSpan (brainspan.org) and PsychENCODE (development.psychencode.org, evolution.psychencode.org) human and macaque RNA-seq data[15,20]. The RNA-seq data consisted of tissue-level samples comprising the pial surface, marginal zone, cortical plate (layers 2–6) and adjacent subplate zone, of eleven prospective neocortical areas. Red and blue lines indicate human and macaque PFC *CBLN2* expression, respectively, and dotted lines represent the non-PFC *CBLN2* expression. Vertical grey box demarcates mid-fetal developmental periods. Predicted ages, timeline of human and macaque development and the associated periods are shown below. Visual representation

of *CBLN2* in human cortex with heatmaps of regional expression in human and macaque below during period 4–6 (**b**) and period 12–13 (**c**). Darker reds represent high expression levels. **d,** Anteroposterior visual representation of human *CBLN2* expression at PCW 21 from the BrainSpan human prenatal laser microdissection microarray data (brainspan.org)[37].

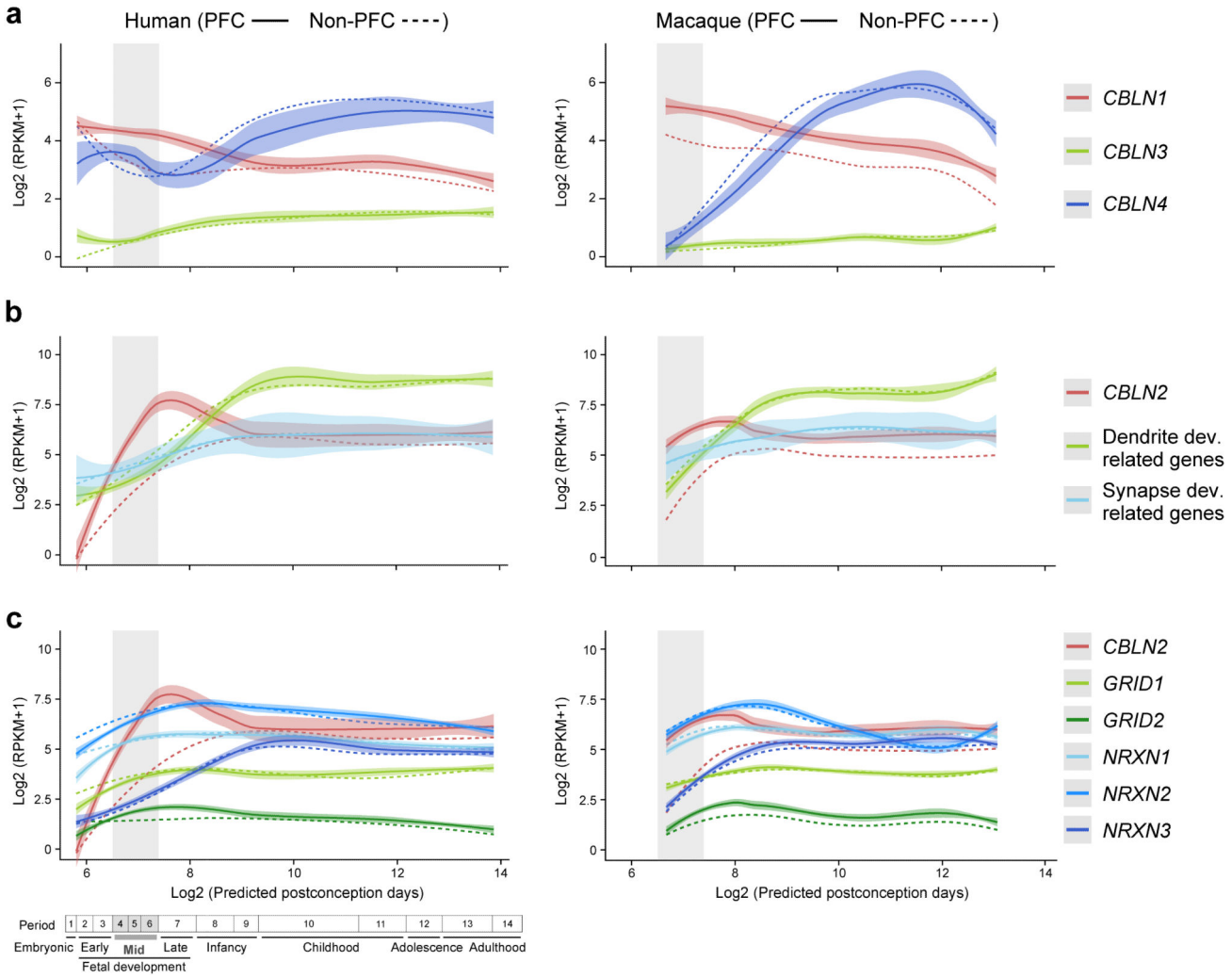

Extended Data Fig. 2 |. Expression profile of *Cbln1,3,4* genes related to dendrite and synapse development and CBLN2 binding partners in macaque and human.

a, Developmental trajectory of *CBLN2* expression compared to the expression of key genes related to dendrite development (i.e., *MAP1A* and *CAMK2A*) and synapse development genes (i.e., *SYP*, *SYPL1*, *SYPL2* and *SYN1*). The lists of genes related to synapse and dendrite development were previously complied and analyzed for their expression trajectories by Kang et al.[35] **b,** Developmental trajectory of *CBLN2* expression compared to the expression of genes encoding CBLN2 binding partners (i.e., *GRID1*, *GRID2*, *NRXN1*, *NRXN2* and *NRXN3*). Left and right panels show gene expression in human and macaque, respectively. Gene expression in PFC and non-PFC are indicated by solid and dashed line, respectively. Vertical grey box highlights the mid-fetal developmental periods. Predicted ages, timeline of human and macaque development and the associated periods are shown

below. Gene expression values are represented as log2(RPKM+1). For all of these plots, the shading around the lines represents the 95% confidence interval. Abbreviations were as described in Fig. 1 legend.

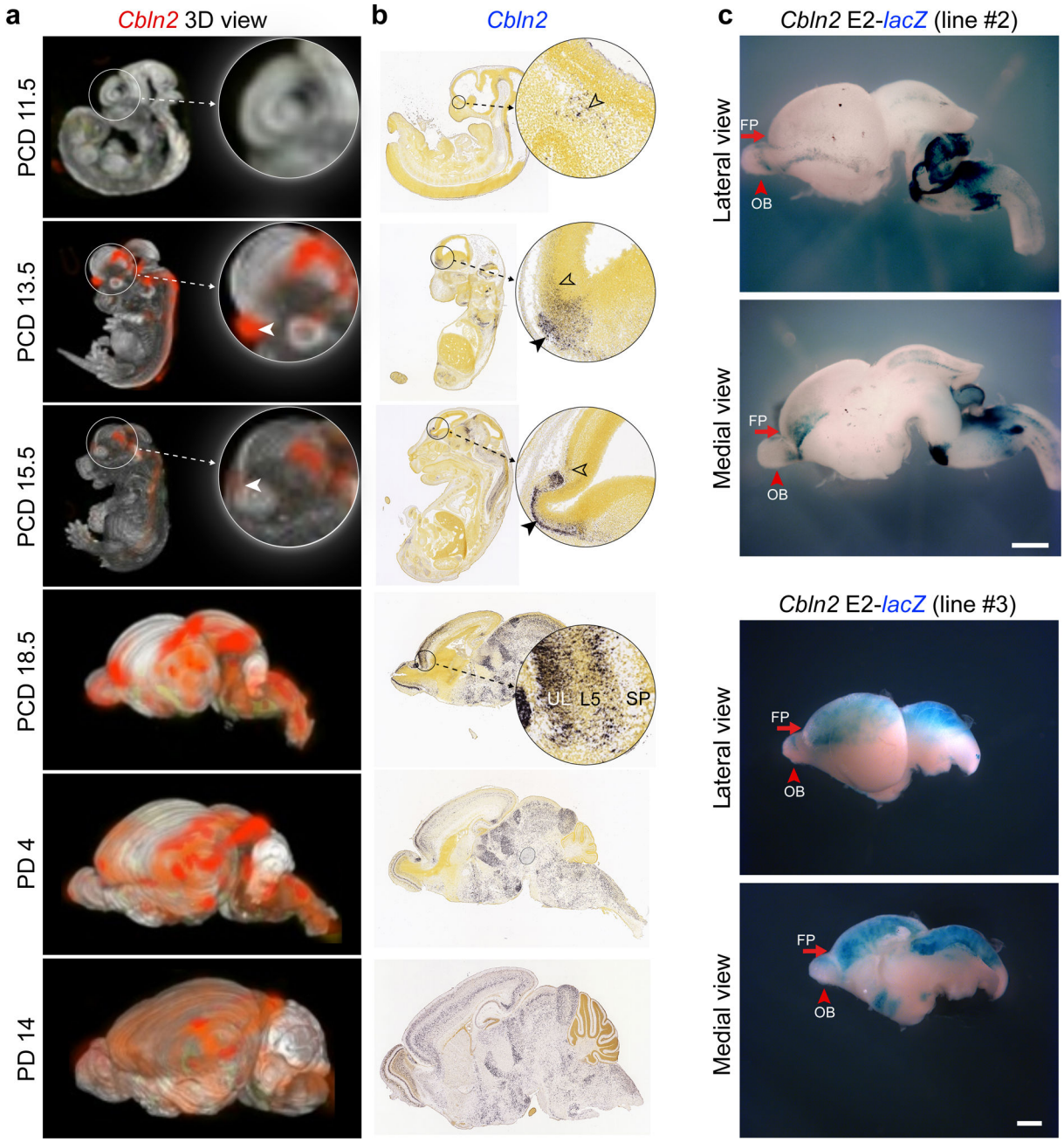

Extended Data Fig. 3 |. Mouse *Cbln2* expression at multiple stages and Cbln2 E2 transgenic lines. Visualization of *Cbln2* expression in wholemount **(a)** and sagittal sections **(b)** at PCD 11.5, 13.5, 15.5 18.5 and PD 4, 14 from Allen Brain Atlas developing mouse brain atlas (developingmouse.brain-map.org) [71]. Arrowheads highlight early rostral expression, UL, upper layer; L5, layer 5; SP, subplate. **c,** β-Galactosidase activity in two additional mouse brains from independent transgenic mouse carrying *Cbln2* E2 conjugated with *lacZ* reporter

at PCD 17. See Fig. 1c for the third replicate. FP, frontal pole; OB, olfactory bulb. Scale bars, 1 mm.

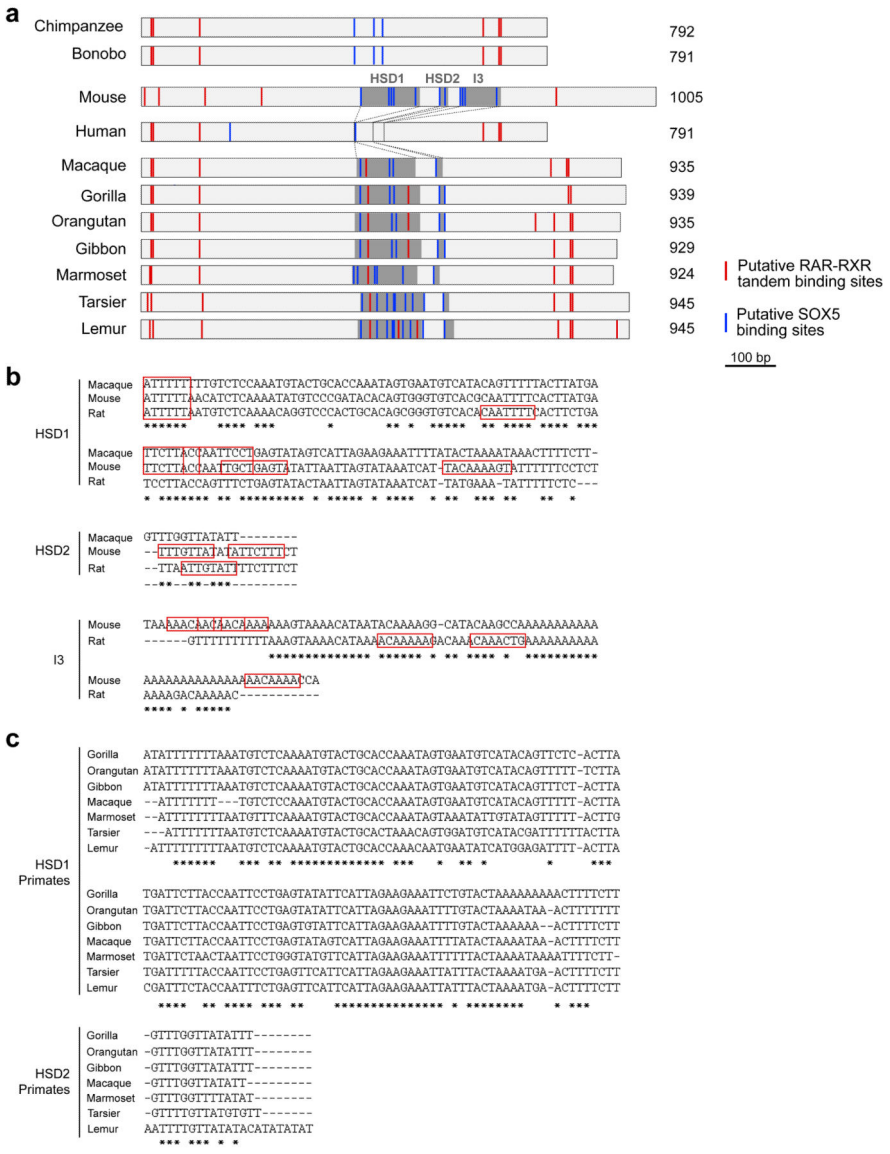

Extended Data Fig. 4 |. Comparative analysis of *CBLN2* E2 deletions across mammals.
a, Schematic representation of *CBLN2* E2 from mouse and primate species including apes (human, common chimpanzee, bonobo, gorilla, orangutan and gibbon), old world monkey (Rhesus macaque), new world monkey (marmoset) and prosimians (tarsier and lemur). HSD1, HSD2 and I3 are shaded. Putative RAR-RXR tandem binding sites indicated as red lines and putative SOX5-binding sites as blue lines. **b,** Sequence alignments of HSD1, HSD2 and I3 from macaque, mouse, and rat. Putative SOX5 binding sites are shown in red boxes. **c,** Sequence alignments of HSD1 and HSD2 from primates shown in (**a**).

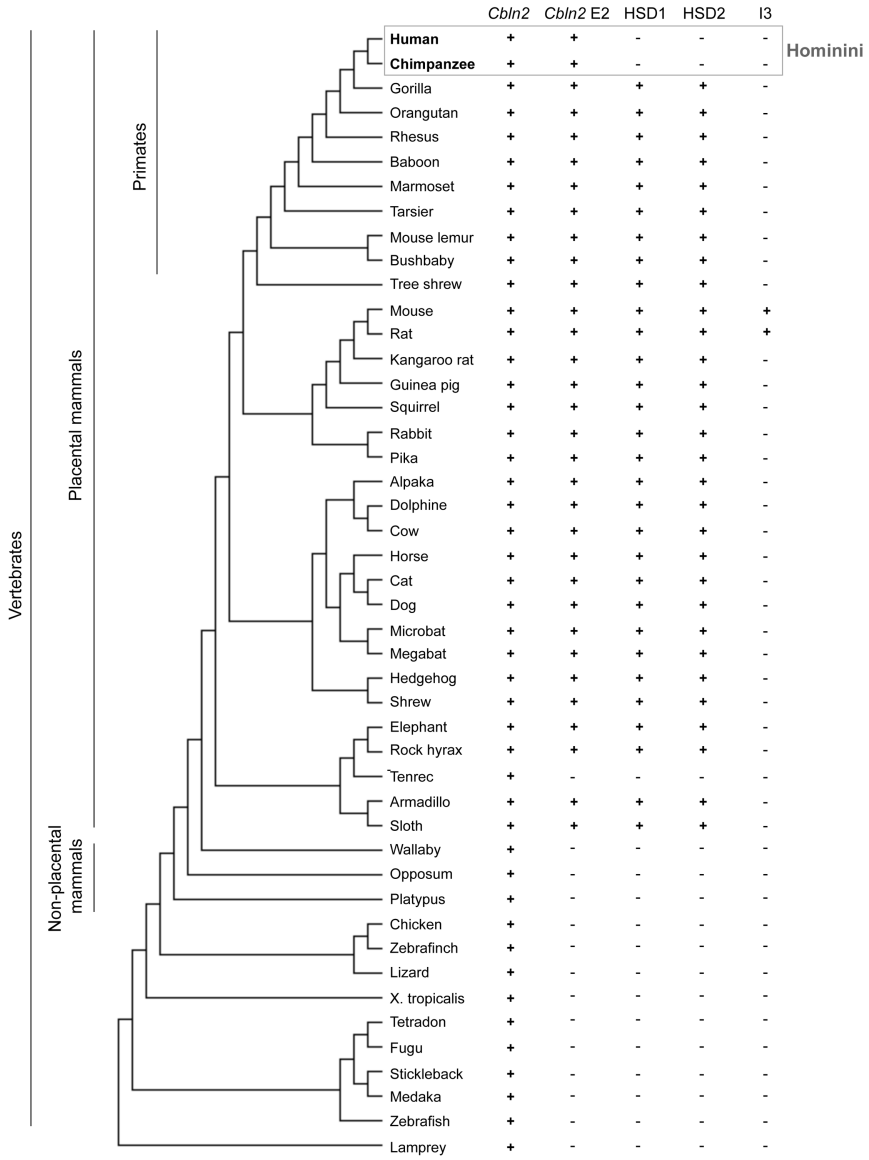

Extended Data Fig. 5 |. Conservation of *CBLN2* E2 and deleted regions across species.

Phylogenetic tree of selected chordates including placental and non-placental mammals with information about presence of the *CBLN2/Cbln2* gene and *CBLN2* E2/Cbln2 E2. The last three columns describe the presence of HSD1, HSD2 and I3. The mouse E2 sequence was searched in each most updated animal genome browser at UCSC genome browser (as of December 22, 2019). E2 conservation criteria are: 1) identity over 80%; and 2) alignment length over 600 bp compared with mouse E2 (1005 bp).

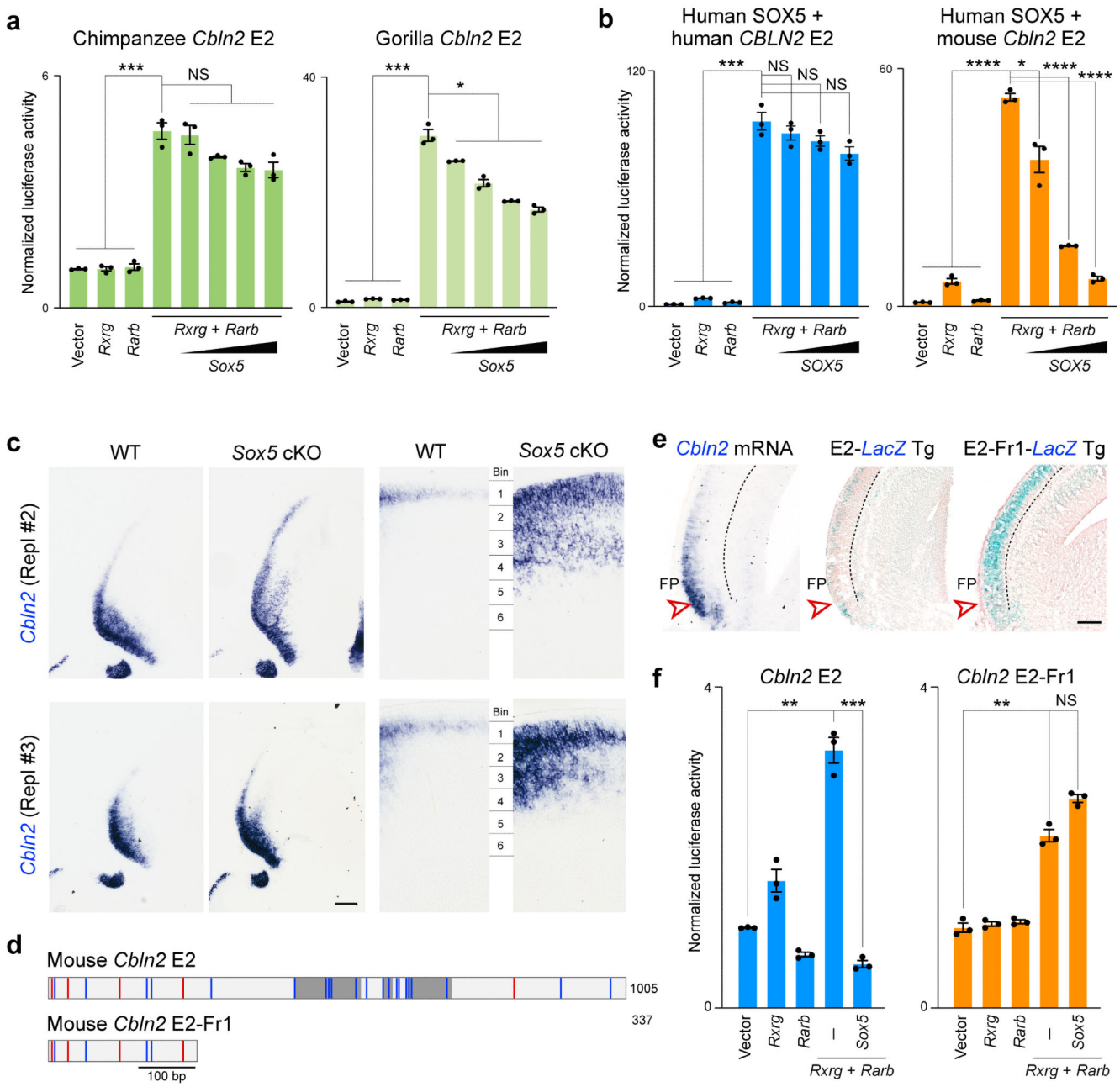

Extended Data Fig. 6 |. SOX5 directly suppresses RXRG-RARB responsive human, chimpanzee, gorilla and mouse *Cbln2* E2 enhancer.

a, Luciferase assay in Neuro-2a cell line from luciferase reporters conjugated to chimpanzee and gorilla wild *Cbln2* E2. Two-tailed Student's t-test; *P = 0.01; ***P = 9e-5 (Chimpanzee), 1e-5 (Gorilla); NS, not significant. Error bars; S.E.M.; N = 3 per condition. **b,** Overexpression of human *SOX5* exerts a similar effect to mouse *Sox5* on human and mouse *Cbln2* E2 reporters. Two-tailed Student's t-test; *P = 5e-3; ***P = 4e-5; ****P = 2e-6; 2e-6, 1e-6 (Human Sox5 + mouse *Cbln2* E2); NS, not significant; Error bars, S.E.M.; N = 3 per condition. **c,** *Cbln2* expression is upregulated in *Sox5* conditional knockout brain at PD 0. Additional two replicates (Repl #2 and 3) not shown in Fig. 2d are shown. Scale

bar, 200 μm (left); 100 μm (right). **d,** Constructs used for luciferase assay and generation of transgenic animals shown in e,f. **e,** Transgenic mouse brain at PCD 17 carrying *Cbln2* E2 (N = 3) or *Cbln2* E2 Fr1-*lacZ* reporters (N = 3). *Cbln2* expression in the PFC is indicated by arrowheads. Endogenous *Cbln2* expression is also shown for comparison (N = 4). Scale bar, 200 μm. **f,** Luciferase assay for *Cbln2* E2 and *Cbln2* E2-Fr1. Two-tailed Student's t-test; **P = 1e-4 (Cbln2 E2), 2e-4 (Cbln2 E2-Fr1); ***P = 8e-5; NS, not significant; Error bars: S.E.M.; N = 3 per condition.

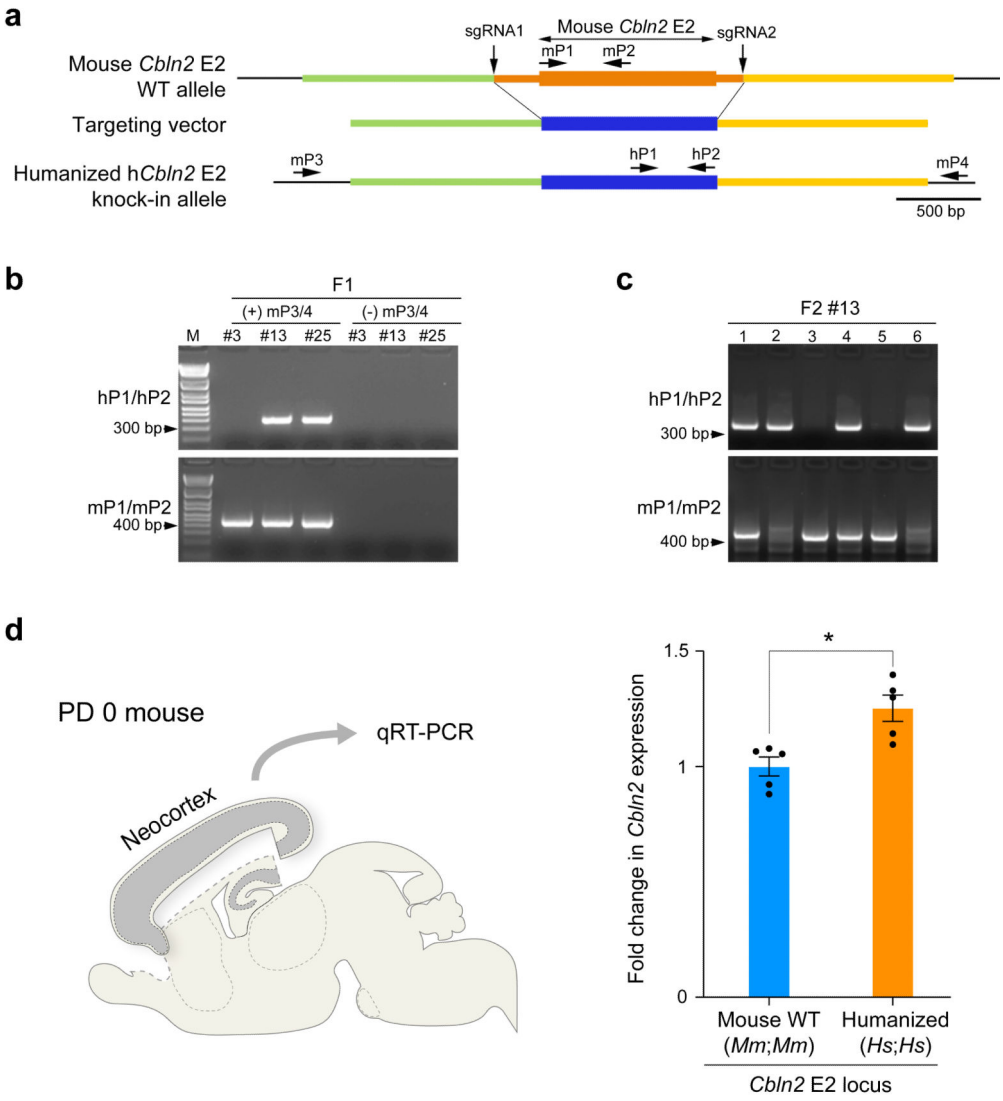

Extended Data Fig. 7 |. Humanized *Cbln2* E2 knock-in mouse shows increased *Cbln2* expression in neonatal neocortex.

a, Positions of single-guide RNAs (sgRNA1 and 2) to introduce double-strand breaks in the genomic DNA and targeting vector to replace WT mouse *Cbln2* E2 region with that of human *CBLN2* E2 (humanized h*Cbln2* E2) are shown. **b**, Genotyping strategy for F1 mice. Germline transmission in the F1 generation was confirmed by nested PCR using the primer set of mP3/mP4, followed by hP1/P2 as indicated in (**a**). Two founders #13 and #25 were

obtained. **c**, Mice in the following generation were genotyped by PCR with hP1/P2 and mP1/mP2. An example of genotyping for F2 of line #13 mice is shown (**c**). **d,** Comparison of *Cbln2* expression between WT *Cbln2* E2 (*Mm;Mm*) and h*Cbln2* E2 (*Hs;Hs*) neocortex at PD 0 using quantitative reverse transcription-PCR. RNA was extracted from the neocortex following the removal of hippocampus, olfactory bulb and subpallial regions. Two-tailed Student's t-test; *P = 0.007; Error bars: S.E.M.; N = 5 per genotype. Genotyping were repeated at least two times in b and c.

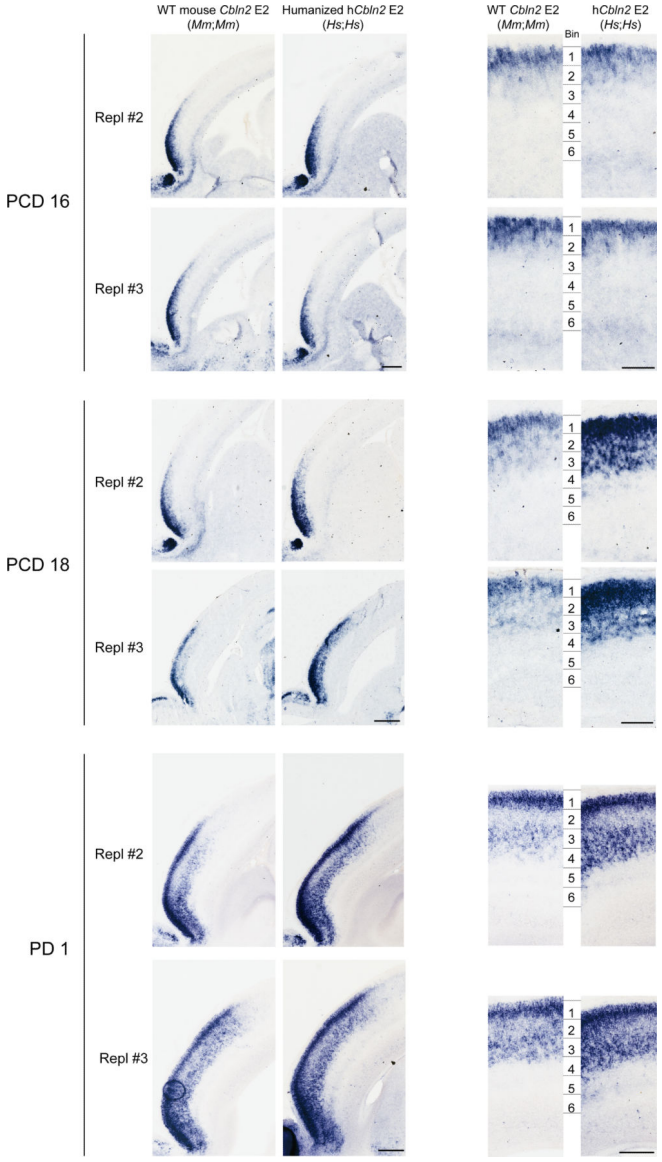

Extended Data Fig. 8 |. Additional replicates from Fig. 3.

The neocortex of the humanized h*Cbln2* E2 knock-in prenatal and neonatal mice exhibits upregulated *Cbln2* in both upper and deeper layers compared to mice carrying WT *Cbln2* E2. Additional two replicates (Repl #2 and 3) not shown in Fig. 3a are shown for PND 16 and PND18. Scale bars, 200 μm (left); 100 μm (right). All analysis and three replicates for

PD1. Neocortex was divided into six equal bins spanning from pia to ventricular zone, and *Cbln2* signal intensity was quantified for each bin and compared between WT and h*Cbln2* E2 (*Hs;Hs*). Two-tailed Student's t-test; *P = 0.02 (PCD18), 0.02, 0.04 (PD1), **P = 1e-3 (PCD18), 1e-3, 3e-3, 3e-3 (PD1), ***P = 1e-4, 2e-4 (PCD18); N = 3 per genotype. Scale bars, 100 μm. **c,** Expression of the upper layer marker, *Cux2,* and SOX5 in adjacent tissue sections were detected by *in situ* hybridization and immunostaining, respectively. Scale bars, 100 μm. N = 3.

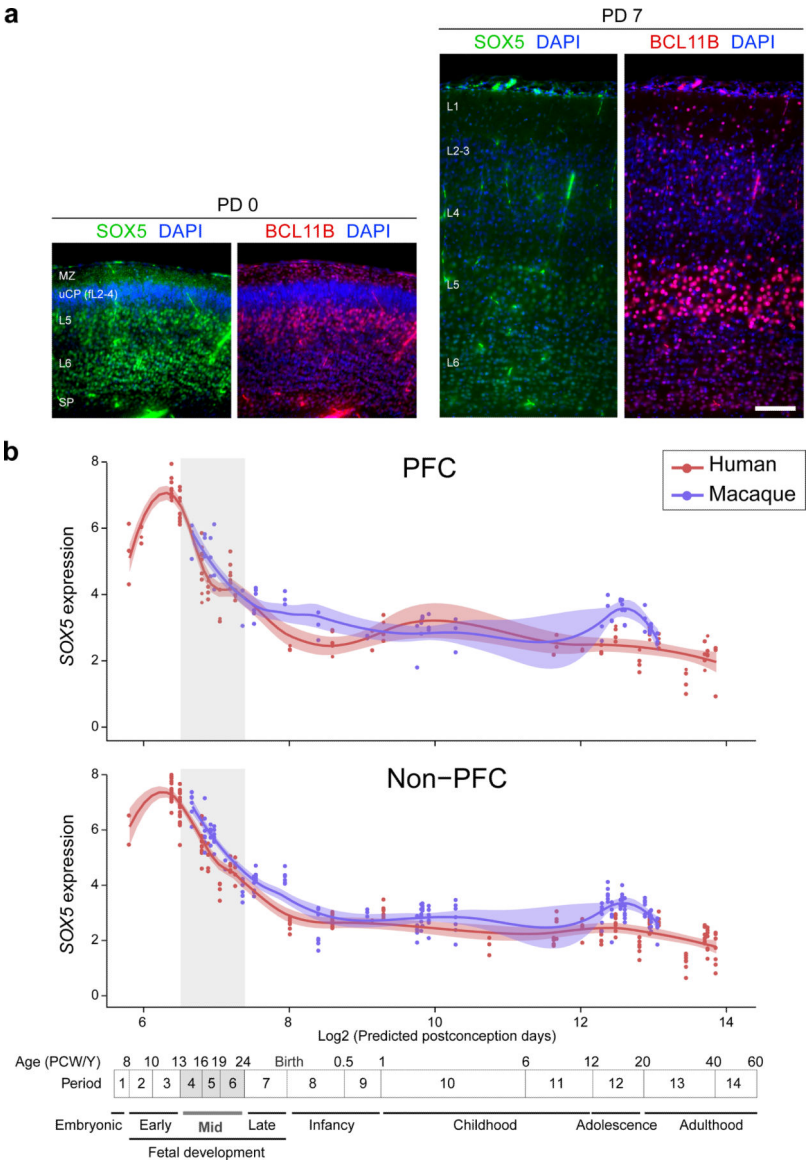

Extended Data Fig. 9 |. Expression of *Sox5* in the developing mouse and human neocortex. **a,** Double immunofluorescent staining for SOX5 and BCL11B in PD 0 and PD 7 mouse neocortex. N = 3 per condition. Scale bar, 100 μm. **b,** SOX5 expression in the PFC and non-PFC areas of the cerebral cortex of human and macaque across development. Red and blue lines indicate human and macaque, respectively. Vertical grey box demarcates mid-fetal

developmental periods. For all of those plots, the shading around the lines represents the 95% confidence interval. Predicted ages, timeline of human and macaque development and the associated periods are shown below.

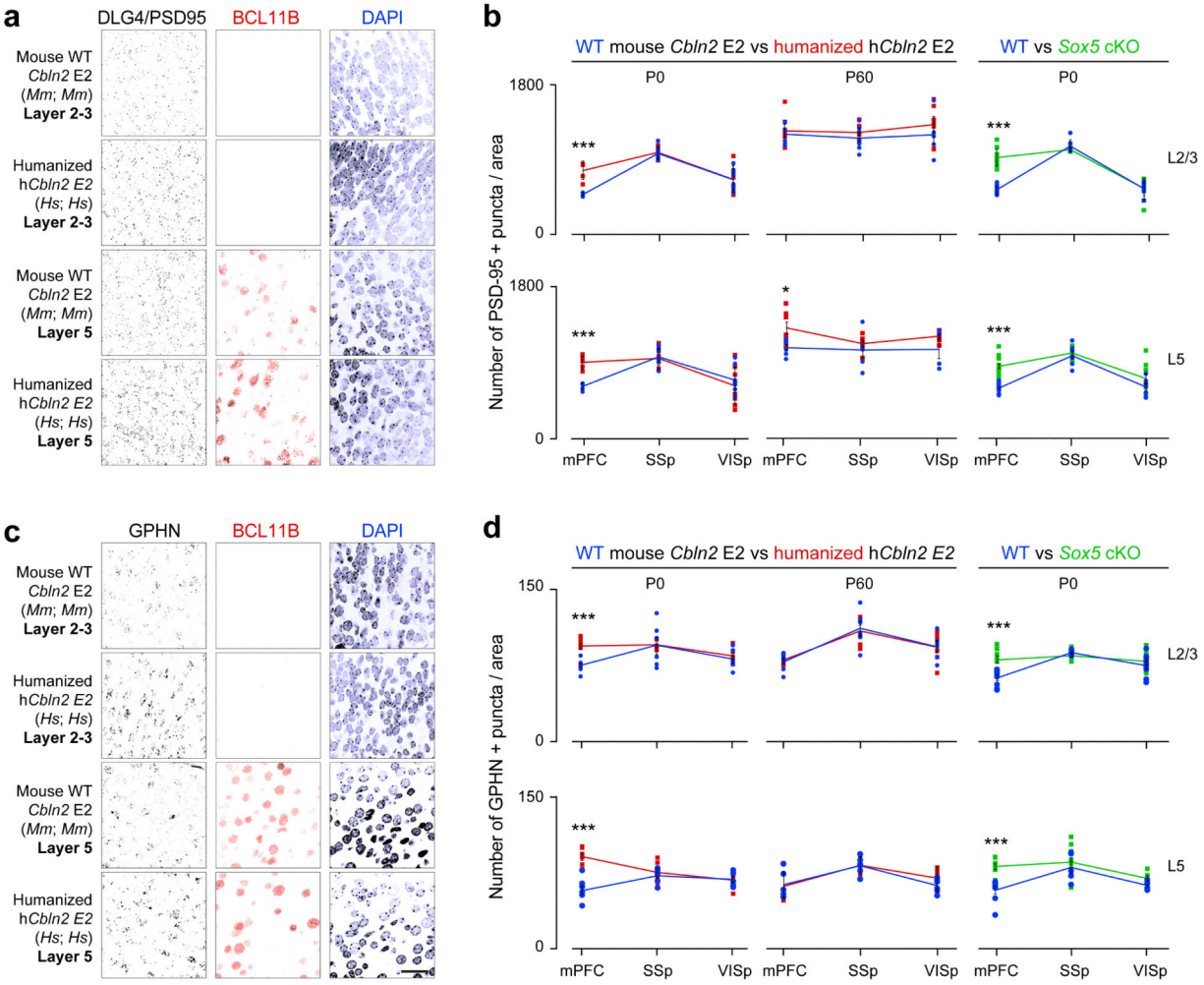

Extended Data Fig. 10 |. Quantification of excitatory and inhibitory postsynaptic puncta

a-d, PD 0 WT and h*Cbln2* E2 mPFC L2-3 and L5 (BCL11B-immunopositive) immunostained for PSD-95/DLG4 or GPHN. Density of PSD-95/DLG4+ excitatory and GPHN+ inhibitory postsynaptic puncta in PD 0 and PD 60 mPFC, primary somatosensory area (SSp), and primary visual area (VISp) of WT (blue), h*Cbln2* E2 (orange), and *Sox5* cKO mice (green). Two-tailed Student's test; *P = 0.018; ***P = 4e-4, 1e-4 (b, WT vs. humanized hCbln2 E2 L2-3, and L5, respectively), 1e-4, 7e-5, 4e-4, 2e-4 (d, WT vs. humanized hCbln2 E2 L2-3 and L5, respectively; WT vs. Sox5 cKO L2-3 and L5, respectively); ****P < 1e-5. Error bars: S.E.M.; N = 5 per PD 0 genotype; N = 3 per PD 60 genotype. Scale bar, 25 μm.

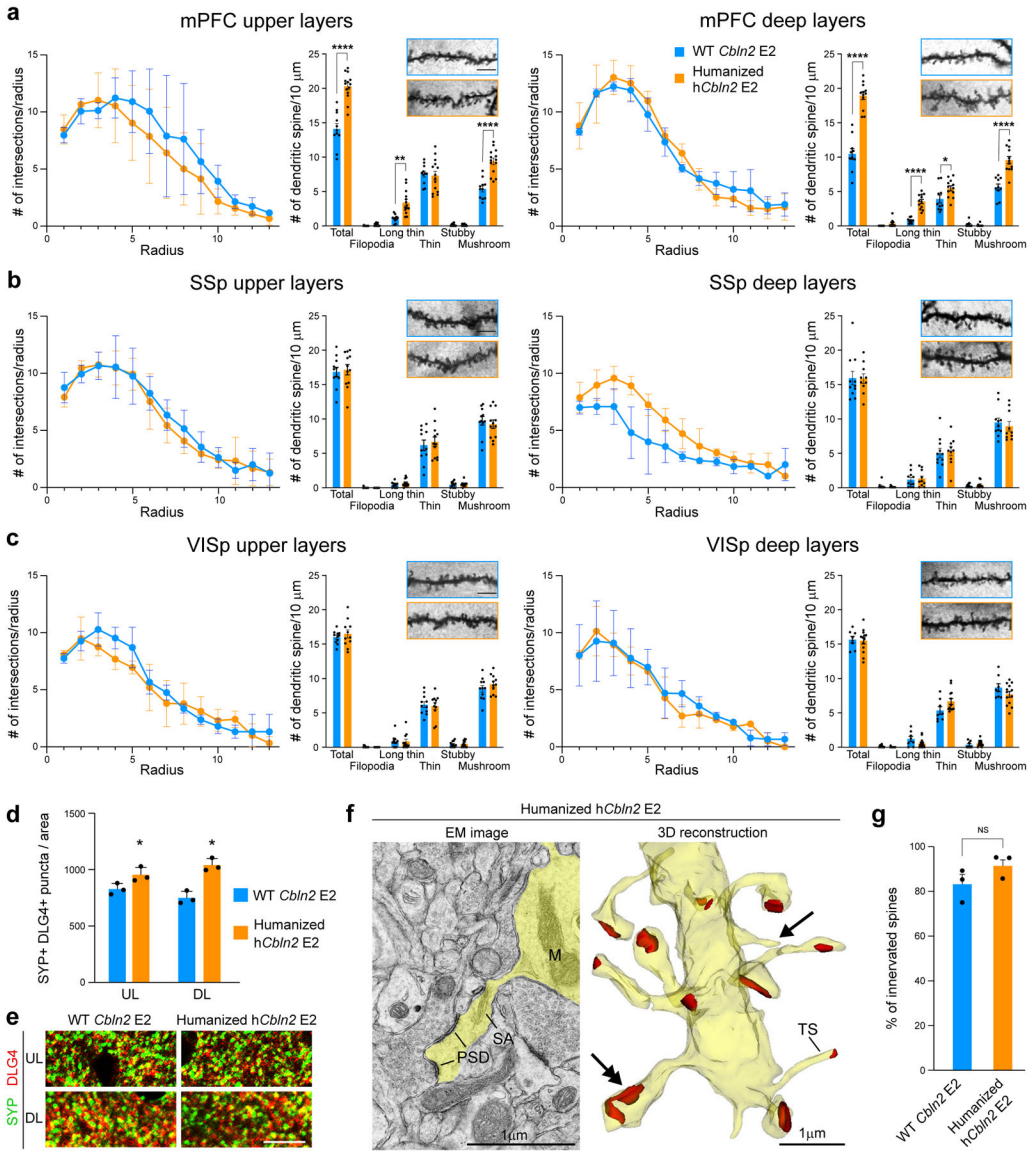

Extended Data Fig. 11 |. Quantification of dendritic spines and dendritic complexity using Golgi stain.

Quantification of Sholl analysis and representative images (inset) of dendritic spines per 10 µm in layer 2–3 and 5 of mPFC (**a**), SSp (**b**) and VISp (**c**) in WT *Cbln2* E2 and humanized hCbln2 E2. Two-way ANOVA with Sidak's multiple comparison method was applied; *P = 0.04; **P = 1e-3, ****P < 0001; Error bars: S.E.M.; N = 16 (WT *Cbln2* E2), and 16 (humanized hCbln2 E2) of PD 60 brains (N = 3). Scale bars: 5 mm. **d,e.** Quantification and representative images of juxtaposed synaptophysin (SYP) and DLG4/PSD-95 immunolabelled puncta in upper (UL) and deep layer (DL) mPFC of WT *Cbln2* E2 and humanized hCbln2 E2. Two-tailed Student's t-test was applied * P = 0.03; Error bars: S.E.M. (N = 3); Scale bar: 10 mm. **f,** Electron microscopy (EM) image shows dendrite emitting spine with postsynaptic density (PSD) and spine apparatus (SA) (left) in PD 60 humanized hCbln2 E2 mouse. 3D reconstruction (right) of the dendrite with numerous spines showing spine heads and synaptic contacts (red). Double arrow points to the spine

shown in EM image. Thin spines without head (TS) and not innervated thin extensions (arrow) are also detected. Abbreviation: M, mitochondria. Sixteen-representable dendrite fragments were traced in the serial images (see Methods). **g,** Quantification of percentage of innervated spines in mPFC of WT *Cbln2* E2 and humanized hCbln2 E2. Two-tailed Student's t-test was applied. NS, Not significant. Error bars: S.E.M. (N =3)

Extended Data Table 1:

Comparative analysis of the transcription factor binding sites in human CBLN2 E2

TF	TF_ID	Chromosome	Start(hg38)	End (hg38)	Primate	Euarchontoglires	Laurasiatheria	Afrotheria	Mars
IRF2	MA0051.1	chr18	72530577	72530594	NO	NO	NO	NO	NO
NFATC2	MA0152.1	chr18	72530837	72530843	NO	NO	NO	NO	NO
STAT1::STAT2	MA0517.1	chr18	72530800	72530814	NO	NO	NO	NO	NO
IRF2	MA0051.1	chr18	72530577	72530594	NO	NO	NO	NO	NO
Stat3	MA0144.1	chr18	72530809	72530818	NO	NO	NO	NO	NO
NFATC2	MA0152.1	chr18	72530837	72530843	NO	NO	NO	NO	NO
STAT1::STAT2	MA0517.1	chr18	72530800	72530814	NO	NO	NO	NO	NO
REL	MA0101.1	chr18	72530715	72530724	YES	NO	NO	NO	NO
NFKB1	MA0105.4	chr18	72530712	72530724	YES	NO	NO	NO	NO
NFKB1	MA0105.4	chr18	72530712	72530724	YES	NO	NO	NO	NO
NFKB1	MA0105.4	chr18	72530713	72530725	YES	NO	NO	NO	NO
RELA	MA0107.1	chr18	72530715	72530724	YES	NO	NO	NO	NO
FOXA1	MA0148.3	chr18	72530538	72530552	YES	NO	NO	NO	NO
FOXP1	MA0481.1	chr18	72530539	72530553	YES	NO	NO	NO	NO
HNF4G	MA0484.1	chr18	72531272	72531286	YES	NO	NO	NO	NO
Nkx2-5(var.2)	MA0503.1	chr18	72530508	72530518	YES	NO	NO	NO	NO
SREBF1	MA0595.1	chr18	72530513	72530522	YES	NO	NO	NO	NO
NFAT5	MA0606.1	chr18	72531082	72531091	YES	NO	NO	NO	NO
NFATC1	MA0624.1	chr18	72531082	72531091	YES	NO	NO	NO	NO
NFATC3	MA0625.1	chr18	72531082	72531091	YES	NO	NO	NO	NO
GCM1	MA0646.1	chr18	72530780	72530790	YES	NO	NO	NO	NO
NFKB2	MA0778.1	chr18	72530712	72530724	YES	NO	NO	NO	NO
NFKB2	MA0778.1	chr18	72530712	72530724	YES	NO	NO	NO	NO
NFKB2	MA0778.1	chr18	72530713	72530725	YES	NO	NO	NO	NO
FOXC2	MA0846.1	chr18	72530540	72530551	YES	NO	NO	NO	NO
BSX	MA0876.1	chr18	72531261	72531268	YES	NO	NO	NO	NO
TFAP2A	MA0003.2	chr18	72531273	72531287	YES	NO	NO	NO	NO
NR2F1	MA0017.1	chr18	72531264	72531277	YES	NO	NO	NO	NO
TEAD1	MA0090.1	chr18	72530683	72530694	YES	NO	NO	NO	NO
REL	MA0101.1	chr18	72530715	72530724	YES	NO	NO	NO	NO
NFKB1	MA0105.2	chr18	72530714	72530724	YES	NO	NO	NO	NO
NFKB1	MA0105.3	chr18	72530714	72530724	YES	NO	NO	NO	NO
NFKB1	MA0105.4	chr18	72530712	72530724	YES	NO	NO	NO	NO
NFKB1	MA0105.4	chr18	72530712	72530724	YES	NO	NO	NO	NO

TF	TF_ID	Chromosome	Start(hg38)	End (hg38)	Primate	Euarchontoglires	Laurasiatheria	Afrotheria	Mars
NFKB1	MA0105.4	chr18	72530713	72530725	YES	NO	NO	NO	NO
RELA	MA0107.1	chr18	72530715	72530724	YES	NO	NO	NO	NO
HNF4A	MA0114.2	chr18	72531271	72531285	YES	NO	NO	NO	NO
FOXA1	MA0148.1	chr18	72530542	72530552	YES	NO	NO	NO	NO
FOXA1	MA0148.2	chr18	72530542	72530552	YES	NO	NO	NO	NO
FOXA1	MA0148.3	chr18	72530538	72530552	YES	NO	NO	NO	NO
EBF1	MA0154.2	chr18	72531274	72531284	YES	NO	NO	NO	NO
FOXP1	MA0481.1	chr18	72530539	72530553	YES	NO	NO	NO	NO
HNF4G	MA0484.1	chr18	72531272	72531286	YES	NO	NO	NO	NO
Nkx2-5(var.2)	MA0503.1	chr18	72530508	72530518	YES	NO	NO	NO	NO
TFAP2C	MA0524.1	chr18	72531273	72531287	YES	NO	NO	NO	NO
SREBF1	MA0595.1	chr18	72530513	72530522	YES	NO	NO	NO	NO
NFAT5	MA0606.1	chr18	72531082	72531091	YES	NO	NO	NO	NO
NFATC1	MA0624.1	chr18	72531082	72531091	YES	NO	NO	NO	NO
NFATC3	MA0625.1	chr18	72531082	72531091	YES	NO	NO	NO	NO
GCM1	MA0646.1	chr18	72530780	72530790	YES	NO	NO	NO	NO
NFKB2	MA0778.1	chr18	72530712	72530724	YES	NO	NO	NO	NO
NFKB2	MA0778.1	chr18	72530712	72530724	YES	NO	NO	NO	NO
NFKB2	MA0778.1	chr18	72530713	72530725	YES	NO	NO	NO	NO
FOXC2	MA0846.1	chr18	72530540	72530551	YES	NO	NO	NO	NO
BSX	MA0876.1	chr18	72531261	72531268	YES	NO	NO	NO	NO
IRF1	MA0050.2	chr18	72531209	72531229	YES	YES	NO	NO	NO
IRF1	MA0050.2	chr18	72531209	72531229	YES	YES	NO	NO	NO
GATA3	MA0037.2	chr18	72530872	72530879	YES	YES	YES	NO	NO
Stat4	MA0518.1	chr18	72530982	72530995	YES	YES	YES	NO	NO
Hoxa9	MA0594.1	chr18	72531092	72531102	YES	YES	YES	NO	NO
DMRT3	MA0610.1	chr18	72530878	72530888	YES	YES	YES	NO	NO
NFIA	MA0670.1	chr18	72531019	72531028	YES	YES	YES	NO	NO
NFIX	MA0671.1	chr18	72531019	72531027	YES	YES	YES	NO	NO
VAX2	MA0723.1	chr18	72530961	72530968	YES	YES	YES	NO	NO
GATA3	MA0037.2	chr18	72530872	72530879	YES	YES	YES	NO	NO
FEV	MA0156.1	chr18	72530984	72530991	YES	YES	YES	NO	NO
Atoh1	MA0461.1	chr18	72531171	72531178	YES	YES	YES	NO	NO
Stat4	MA0518.1	chr18	72530982	72530995	YES	YES	YES	NO	NO
Hoxa9	MA0594.1	chr18	72531092	72531102	YES	YES	YES	NO	NO
DMRT3	MA0610.1	chr18	72530878	72530888	YES	YES	YES	NO	NO
NFIA	MA0670.1	chr18	72531019	72531028	YES	YES	YES	NO	NO
NFIX	MA0671.1	chr18	72531019	72531027	YES	YES	YES	NO	NO
VAX2	MA0723.1	chr18	72530961	72530968	YES	YES	YES	NO	NO
Nr2f6(var.2)	MA0728.1	chr18	72530603	72530617	YES	NO	NO	YES	NO
CREB3L1	MA0839.1	chr18	72530971	72530984	YES	NO	NO	YES	NO
Nr2f6(var.2)	MA0728.1	chr18	72530603	72530617	YES	NO	NO	YES	NO

TF	TF_ID	Chromosome	Start(hg38)	End (hg38)	Primate	Euarchontoglires	Laurasiatheria	Afrotheria	Mars
CREB3L1	MA0839.1	chr18	72530971	72530984	YES	NO	NO	YES	NO
RORA(var.2)	MA0072.1	chr18	72531108	72531121	YES	YES	NO	YES	NO
RORA(var.2)	MA0072.1	chr18	72531108	72531121	YES	YES	NO	YES	NO
PAX5	MA0014.2	chr18	72530928	72530946	YES	NO	YES	YES	NO
PLAG1	MA0163.1	chr18	72530895	72530908	YES	NO	YES	YES	NO
Gfi1b	MA0483.1	chr18	72530761	72530771	YES	NO	YES	YES	NO
POU1F1	MA0784.1	chr18	72530656	72530669	YES	NO	YES	YES	NO
POU2F1	MA0785.1	chr18	72530658	72530669	YES	NO	YES	YES	NO
POU3F1	MA0786.1	chr18	72530657	72530668	YES	NO	YES	YES	NO
POU3F2	MA0787.1	chr18	72530657	72530668	YES	NO	YES	YES	NO
POU3F3	MA0788.1	chr18	72530657	72530669	YES	NO	YES	YES	NO
E2F8	MA0865.1	chr18	72530901	72530912	YES	NO	YES	YES	NO
PAX5	MA0014.2	chr18	72530928	72530946	YES	NO	YES	YES	NO
NR2F1	MA0017.1	chr18	72530603	72530616	YES	NO	YES	YES	NO
PLAG1	MA0163.1	chr18	72530895	72530908	YES	NO	YES	YES	NO
Gfi1b	MA0483.1	chr18	72530761	72530771	YES	NO	YES	YES	NO
TFAP2C	MA0524.1	chr18	72530896	72530910	YES	NO	YES	YES	NO
POU1F1	MA0784.1	chr18	72530656	72530669	YES	NO	YES	YES	NO
POU2F1	MA0785.1	chr18	72530658	72530669	YES	NO	YES	YES	NO
POU3F1	MA0786.1	chr18	72530657	72530668	YES	NO	YES	YES	NO
POU3F2	MA0787.1	chr18	72530657	72530668	YES	NO	YES	YES	NO
POU3F3	MA0788.1	chr18	72530657	72530669	YES	NO	YES	YES	NO
E2F8	MA0865.1	chr18	72530901	72530912	YES	NO	YES	YES	NO
NR2F1	MA0017.2	chr18	72530599	72530611	YES	YES	YES	YES	NO
CREB1	MA0018.2	chr18	72530603	72530610	YES	YES	YES	YES	NO
Gfi1	MA0038.1	chr18	72530771	72530780	YES	YES	YES	YES	NO
RORA	MA0071.1	chr18	72530603	72530612	YES	YES	YES	YES	NO
SOX9	MA0077.1	chr18	72530577	72530585	YES	YES	YES	YES	NO
RELA	MA0107.1	chr18	72530714	72530723	YES	YES	YES	YES	NO
RELA	MA0107.1	chr18	72530714	72530723	YES	YES	YES	YES	NO
CTCF	MA0139.1	chr18	72530784	72530802	YES	YES	YES	YES	NO
Pou5f1::Sox2	MA0142.1	chr18	72530745	72530759	YES	YES	YES	YES	NO
Gfi1b	MA0483.1	chr18	72530772	72530782	YES	YES	YES	YES	NO
Gfi1b	MA0483.1	chr18	72531134	72531144	YES	YES	YES	YES	NO
Hoxc9	MA0485.1	chr18	72531091	72531103	YES	YES	YES	YES	NO
POU2F2	MA0507.1	chr18	72530656	72530668	YES	YES	YES	YES	NO
POU2F2	MA0507.1	chr18	72530742	72530754	YES	YES	YES	YES	NO
SMAD2::SMAD3::SMAD4	MA0513.1	chr18	72531140	72531152	YES	YES	YES	YES	NO
EMX1	MA0612.1	chr18	72530960	72530969	YES	YES	YES	YES	NO
Pou2f3	MA0627.1	chr18	72530655	72530670	YES	YES	YES	YES	NO
MYF6	MA0667.1	chr18	72530817	72530826	YES	YES	YES	YES	NO

TF	TF_ID	Chromosome	Start(hg38)	End (hg38)	Primate	Euarchontoglires	Laurasiatheria	Afrotheria	Mars
MYF6	MA0667.1	chr18	72530817	72530826	YES	YES	YES	YES	NO
POU1F1	MA0784.1	chr18	72530742	72530755	YES	YES	YES	YES	NO
POU3F4	MA0789.1	chr18	72530659	72530667	YES	YES	YES	YES	NO
POU5F1B	MA0792.1	chr18	72530659	72530667	YES	YES	YES	YES	NO
TFAP2B(var.2)	MA0812.1	chr18	72530897	72530907	YES	YES	YES	YES	NO
BARX1	MA0875.1	chr18	72530922	72530929	YES	YES	YES	YES	NO
EVX1	MA0887.1	chr18	72530960	72530969	YES	YES	YES	YES	NO
EVX2	MA0888.1	chr18	72530960	72530969	YES	YES	YES	YES	NO
HOXA2	MA0900.1	chr18	72530960	72530969	YES	YES	YES	YES	NO
HOXB2	MA0902.1	chr18	72530960	72530969	YES	YES	YES	YES	NO
HOXB3	MA0903.1	chr18	72530960	72530969	YES	YES	YES	YES	NO
NR2F1	MA0017.2	chr18	72530599	72530611	YES	YES	YES	YES	NO
CREB1	MA0018.2	chr18	72530603	72530610	YES	YES	YES	YES	NO
Gfi1	MA0038.1	chr18	72530771	72530780	YES	YES	YES	YES	NO
RORA	MA0071.1	chr18	72530603	72530612	YES	YES	YES	YES	NO
SOX9	MA0077.1	chr18	72530577	72530585	YES	YES	YES	YES	NO
NFKB1	MA0105.1	chr18	72530714	72530723	YES	YES	YES	YES	NO
NFKB1	MA0105.1	chr18	72530714	72530723	YES	YES	YES	YES	NO
NFKB1	MA0105.2	chr18	72530713	72530723	YES	YES	YES	YES	NO
NFKB1	MA0105.3	chr18	72530713	72530723	YES	YES	YES	YES	NO
RELA	MA0107.1	chr18	72530714	72530723	YES	YES	YES	YES	NO
RELA	MA0107.1	chr18	72530714	72530723	YES	YES	YES	YES	NO
ESR1	MA0112.2	chr18	72531144	72531163	YES	YES	YES	YES	NO
ELF5	MA0136.1	chr18	72530983	72530991	YES	YES	YES	YES	NO
CTCF	MA0139.1	chr18	72530784	72530802	YES	YES	YES	YES	NO
Pou5f1::Sox2	MA0142.1	chr18	72530745	72530759	YES	YES	YES	YES	NO
Atoh1	MA0461.1	chr18	72531105	72531112	YES	YES	YES	YES	NO
Gfi1b	MA0483.1	chr18	72530772	72530782	YES	YES	YES	YES	NO
Gfi1b	MA0483.1	chr18	72531134	72531144	YES	YES	YES	YES	NO
Hoxc9	MA0485.1	chr18	72531091	72531103	YES	YES	YES	YES	NO
POU2F2	MA0507.1	chr18	72530656	72530668	YES	YES	YES	YES	NO
POU2F2	MA0507.1	chr18	72530742	72530754	YES	YES	YES	YES	NO
SMAD2::SMAD3::SMAD4	MA0513.1	chr18	72531140	72531152	YES	YES	YES	YES	NO
EMX1	MA0612.1	chr18	72530960	72530969	YES	YES	YES	YES	NO
Pou2f3	MA0627.1	chr18	72530655	72530670	YES	YES	YES	YES	NO
MYF6	MA0667.1	chr18	72530817	72530826	YES	YES	YES	YES	NO
MYF6	MA0667.1	chr18	72530817	72530826	YES	YES	YES	YES	NO
POU1F1	MA0784.1	chr18	72530742	72530755	YES	YES	YES	YES	NO
POU3F4	MA0789.1	chr18	72530659	72530667	YES	YES	YES	YES	NO
POU5F1B	MA0792.1	chr18	72530659	72530667	YES	YES	YES	YES	NO

TF	TF_ID	Chromosome	Start(hg38)	End (hg38)	Primate	Euarchontoglires	Laurasiatheria	Afrotheria	Mars
TFAP2B(var.2)	MA0812.1	chr18	72530897	72530907	YES	YES	YES	YES	NO
BARX1	MA0875.1	chr18	72530922	72530929	YES	YES	YES	YES	NO
EVX1	MA0887.1	chr18	72530960	72530969	YES	YES	YES	YES	NO
EVX2	MA0888.1	chr18	72530960	72530969	YES	YES	YES	YES	NO
HOXA2	MA0900.1	chr18	72530960	72530969	YES	YES	YES	YES	NO
HOXB2	MA0902.1	chr18	72530960	72530969	YES	YES	YES	YES	NO
HOXB3	MA0903.1	chr18	72530960	72530969	YES	YES	YES	YES	NO
TFAP2A	MA0003.1	chr18	72530721	72530729	YES	YES	YES	NO	YES
Pax4	MA0068.1	chr18	72530970	72530999	YES	YES	YES	NO	YES
TFAP2A	MA0003.3	chr18	72530897	72530907	YES	YES	YES	YES	YES
Gfi1	MA0038.1	chr18	72531133	72531142	YES	YES	YES	YES	YES
Foxd3	MA0041.1	chr18	72530816	72530827	YES	YES	YES	YES	YES
TFAP2C	MA0524.2	chr18	72530897	72530908	YES	YES	YES	YES	YES
Pou2f3	MA0627.1	chr18	72530741	72530756	YES	YES	YES	YES	YES
POU2F1	MA0785.1	chr18	72530744	72530755	YES	YES	YES	YES	YES
POU3F4	MA0789.1	chr18	72530745	72530753	YES	YES	YES	YES	YES
POU5F1B	MA0792.1	chr18	72530745	72530753	YES	YES	YES	YES	YES
TFAP2A(var.2)	MA0810.1	chr18	72530897	72530908	YES	YES	YES	YES	YES
TFAP2B	MA0811.1	chr18	72530897	72530908	YES	YES	YES	YES	YES
Barhl1	MA0877.1	chr18	72530921	72530930	YES	YES	YES	YES	YES
TFAP2A	MA0003.2	chr18	72530894	72530908	YES	YES	YES	YES	YES
TFAP2A	MA0003.3	chr18	72530897	72530907	YES	YES	YES	YES	YES
Gfi1	MA0038.1	chr18	72531133	72531142	YES	YES	YES	YES	YES
Foxd3	MA0041.1	chr18	72530816	72530827	YES	YES	YES	YES	YES
Foxa2	MA0047.1	chr18	72530816	72530827	YES	YES	YES	YES	YES
TFAP2C	MA0524.2	chr18	72530897	72530908	YES	YES	YES	YES	YES
Pou2f3	MA0627.1	chr18	72530741	72530756	YES	YES	YES	YES	YES
POU2F1	MA0785.1	chr18	72530744	72530755	YES	YES	YES	YES	YES
POU3F4	MA0789.1	chr18	72530745	72530753	YES	YES	YES	YES	YES
POU5F1B	MA0792.1	chr18	72530745	72530753	YES	YES	YES	YES	YES
TFAP2A(var.2)	MA0810.1	chr18	72530897	72530908	YES	YES	YES	YES	YES
TFAP2B	MA0811.1	chr18	72530897	72530908	YES	YES	YES	YES	YES
Barhl1	MA0877.1	chr18	72530921	72530930	YES	YES	YES	YES	YES
TAL1::TCF3	MA0091.1	chr18	72531153	72531164	YES	YES	YES	NO	NO
TAL1::TCF3	MA0091.1	chr18	72531155	72531166	YES	YES	YES	NO	NO
Stat6	MA0520.1	chr18	72531171	72531185	YES	YES	YES	NO	NO
Bhlha15	MA0607.1	chr18	72531156	72531163	YES	YES	YES	NO	NO
TAL1::TCF3	MA0091.1	chr18	72531153	72531164	YES	YES	YES	NO	NO
TAL1::TCF3	MA0091.1	chr18	72531155	72531166	YES	YES	YES	NO	NO
Stat6	MA0520.1	chr18	72531171	72531185	YES	YES	YES	NO	NO

TF	TF_ID	Chromosome	Start(hg38)	End (hg38)	Primate	Euarchontoglires	Laurasiatheria	Afrotheria	Mars
Bhlha15	MA0607.1	chr18	72531156	72531163	YES	YES	YES	NO	NO
Crx	MA0467.1	chr18	72531051	72531061	YES	YES	YES	YES	NO
Sox3	MA0514.1	chr18	72531015	72531024	YES	YES	YES	YES	NO
LBX1	MA0618.1	chr18	72531113	72531120	YES	YES	YES	YES	NO
POU6F2	MA0793.1	chr18	72531111	72531120	YES	YES	YES	YES	NO
Dmbx1	MA0883.1	chr18	72531049	72531065	YES	YES	YES	YES	NO
GSC2	MA0891.1	chr18	72531053	72531062	YES	YES	YES	YES	NO
Crx	MA0467.1	chr18	72531051	72531061	YES	YES	YES	YES	NO
Sox3	MA0514.1	chr18	72531015	72531024	YES	YES	YES	YES	NO
LBX1	MA0618.1	chr18	72531113	72531120	YES	YES	YES	YES	NO
POU6F2	MA0793.1	chr18	72531111	72531120	YES	YES	YES	YES	NO
Dmbx1	MA0883.1	chr18	72531049	72531065	YES	YES	YES	YES	NO
GSC2	MA0891.1	chr18	72531053	72531062	YES	YES	YES	YES	NO
TAL1::TCF3	MA0091.1	chr18	72531103	72531114	YES	YES	NO	YES	YES
TAL1::TCF3	MA0091.1	chr18	72531103	72531114	YES	YES	NO	YES	YES
TAL1::TCF3	MA0091.1	chr18	72531101	72531112	YES	YES	YES	YES	YES
Atoh1	MA0461.2	chr18	72531103	72531112	YES	YES	YES	YES	YES
mix-a	MA0621.1	chr18	72531112	72531122	YES	YES	YES	YES	YES
Neurog1	MA0623.1	chr18	72531103	72531112	YES	YES	YES	YES	YES
Neurog1	MA0623.1	chr18	72531103	72531112	YES	YES	YES	YES	YES
NEUROD2	MA0668.1	chr18	72531103	72531112	YES	YES	YES	YES	YES
NEUROG2	MA0669.1	chr18	72531103	72531112	YES	YES	YES	YES	YES
VAX1	MA0722.1	chr18	72531113	72531120	YES	YES	YES	YES	YES
VSX1	MA0725.1	chr18	72531113	72531120	YES	YES	YES	YES	YES
VSX2	MA0726.1	chr18	72531113	72531120	YES	YES	YES	YES	YES
Dlx1	MA0879.1	chr18	72531112	72531121	YES	YES	YES	YES	YES
EMX2	MA0886.1	chr18	72531112	72531121	YES	YES	YES	YES	YES
Hoxb5	MA0904.1	chr18	72531108	72531123	YES	YES	YES	YES	YES
Hoxd3	MA0912.1	chr18	72531108	72531123	YES	YES	YES	YES	YES
SP1	MA0079.1	chr18	72530997	72531006	YES	YES	YES	YES	YES
TAL1::TCF3	MA0091.1	chr18	72531101	72531112	YES	YES	YES	YES	YES
Atoh1	MA0461.2	chr18	72531103	72531112	YES	YES	YES	YES	YES
mix-a	MA0621.1	chr18	72531112	72531122	YES	YES	YES	YES	YES
Neurog1	MA0623.1	chr18	72531103	72531112	YES	YES	YES	YES	YES
Neurog1	MA0623.1	chr18	72531103	72531112	YES	YES	YES	YES	YES
NEUROD2	MA0668.1	chr18	72531103	72531112	YES	YES	YES	YES	YES
NEUROG2	MA0669.1	chr18	72531103	72531112	YES	YES	YES	YES	YES
VAX1	MA0722.1	chr18	72531113	72531120	YES	YES	YES	YES	YES
VSX1	MA0725.1	chr18	72531113	72531120	YES	YES	YES	YES	YES
VSX2	MA0726.1	chr18	72531113	72531120	YES	YES	YES	YES	YES
Dlx1	MA0879.1	chr18	72531112	72531121	YES	YES	YES	YES	YES
EMX2	MA0886.1	chr18	72531112	72531121	YES	YES	YES	YES	YES

TF	TF_ID	Chromosome	Start(hg38)	End (hg38)	Primate	Euarchontoglires	Laurasiatheria	Afrotheria	Mars
Hoxb5	MA0904.1	chr18	72531108	72531123	YES	YES	YES	YES	YES
Hoxd3	MA0912.1	chr18	72531108	72531123	YES	YES	YES	YES	YES

** NOTE: Yes means BS is conserved (no mutations in core of motif) in at least 25% of the species in that group/clade.

Extended Data Table 2:

List and sequence of relevant sgRNAs and primers

Oligo name	Use	Sequence
mCbln2 sgRNA-L1-top	sgRNA synthesis	caccgTAAGGCGTGTTGCACAAGAT
mCbln2 sgRNA-L1-bottom	sgRNA synthesis	aaacATCTTGTGCAACACGCCTTAc
mCbln2 sgRNA-R1-top	sgRNA synthesis	caccgATCACAATTTATCTACCGTG
mCbln2 sgRNA-R1-bottom	sgRNA synthesis	aaacCACGGTAGATAAATTGTGATc
T7- mCbln2-sgRNA-L1	sgRNA synthesis	gaaattaatacgactcactatagggagaTAAGGCGTGTTGCACAAGAT
Primer name	**Use**	**Sequence**
T7-mCbln2 sgRNA-R1	sgRNA synthesis	gaaattaatacgactcactatagggagaATCACAATTTATCTACCGTG
mP1	genotyping	GTTGAAATTGATGGTCCAGGTG
mP2	genotyping	AAAATTGCGTGACACCCACT
mP3	genotyping	CAAGCCTTTGGAATGTTGAGCTAC
mP4	genotyping	CCAGAAGTGAAGCCAATGAGAGAA
hP1	genotyping	CCCTAAGGCCTATTACTTT
hP2	genotyping	GAAGGCCTCTCAGCTCATCTTTT
LacZ-F	genotyping	ATCCTCTGCATGGTCAGGTC
LacZ-R	genotyping	CGTGGCCTGATTCATTCC
E2-ChIP-F	ChIP	GTCCCGATACACAGTGGGTG
E2-ChIP-R	ChIP	AGCACCATCTATTGGGGAGG
E1-ChIP-F	ChIP	TGGGACAAGAGAATGTCAGC
E1-ChIP-R	ChIP	GTTACTCAGGACTGAAGCTGAA
qPCR-Cbln2-F	quantitative PCR	TGACCCTCAGATGGATTGCAC
qPCR-Cbln2-R	quantitative PCR	CTGCTGGGCTCTTGCTTTAAGC
qPCR-Tbp-F	quantitative PCR	GTGATGTGAAGTTCCCCATAAGG
qPCR-Tbp-R	quantitative PCR	CTACTGAACTGCTGGTGGGGTCA

Supplementary Material

Refer to Web version on PubMed Central for supplementary material.

Acknowledgements

We thank Suxia Bai, Timothy Nottoli and Xiaojun Xing for technical help with generating transgenic mice and genetically humanized mice; Andre Sousa for providing tissue; Belen Lorente-Galdos and Gabriel Santpere for helping with data analysis; Alvaro Duque for using equipment from MacBrainResource (MH113257); Véronique Lefebvre for providing floxed *Sox5* mice; and the members of the Sestan laboratory for comments. This work was supported by the National Institutes of Health (HG010898, MH106874, MH106934, MH110926, MH116488), and the Simons Foundation (N.S.). Additional support was provided by the National Institutes of Health T32 fellowship

(MH18268) (K.P.), the National Science Foundation Graduate Research Fellowship Program (S.K.M.), the Kavli Foundation and the James S. McDonnell Foundation (N.S.).

References

1. Finlay BL & Darlington RB Linked regularities in the development and evolution of mammalian brains. Science 268, 1578–1584 (1995). [PubMed: 7777856]
2. Barton RA & Harvey PH Mosaic evolution of brain structure in mammals. Nature 405, 1055–1058 (2000). [PubMed: 10890446]
3. Krubitzer L & Kaas J The evolution of the neocortex in mammals: how is phenotypic diversity generated? Curr. Opin. Neurobiol 15, 444–453 (2005). [PubMed: 16026978]
4. Passingham RE & Wise SP The Neurobiology of the Prefrontal Cortex: Anatomy, Evolution, and The Origin of Insight. (Oxford University Press, 2015).
5. Elston GN et al. Specializations of the granular prefrontal cortex of primates: implications for cognitive processing. Anat. Rec. A Discov. Mol. Cell. Evol. Biol 288, 26–35 (2006). [PubMed: 16342214]
6. Semendeferi K et al. Spatial organization of neurons in the frontal pole sets humans apart from great apes. Cereb. Cortex 21, 1485–1497 (2011). [PubMed: 21098620]
7. Kwan KY et al. Species-dependent posttranscriptional regulation of NOS1 by FMRP in the developing cerebral cortex. Cell 149, 899–911 (2012). [PubMed: 22579290]
8. Gabi M et al. No relative expansion of the number of prefrontal neurons in primate and human evolution. Proc. Natl. Acad. Sci. U. S. A 113, 9617–9622 (2016). [PubMed: 27503881]
9. Caceres M et al. Elevated gene expression levels distinguish human from non-human primate brains. Proc. Natl. Acad. Sci. U. S. A 100, 13030–13035 (2003). [PubMed: 14557539]
10. Khaitovich P et al. Regional patterns of gene expression in human and chimpanzee brains. Genome Res. 14, 1462–1473 (2004). [PubMed: 15289471]
11. Uddin M et al. Sister grouping of chimpanzees and humans as revealed by genome-wide phylogenetic analysis of brain gene expression profiles. Proc. Natl. Acad. Sci. U. S. A 101, 2957–2962 (2004). [PubMed: 14976249]
12. Konopka G et al. Human-specific transcriptional networks in the brain. Neuron 75, 601–617 (2012). [PubMed: 22920253]
13. Bauernfeind AL et al. Evolutionary divergence of gene and protein expression in the brains of humans and chimpanzees. Genome Biol Evol 7, 2276–2288 (2015). [PubMed: 26163674]
14. Sousa AMM et al. Molecular and cellular reorganization of neural circuits in the human lineage. Science 358, 1027–1032 (2017). [PubMed: 29170230]
15. Zhu Y et al. Spatiotemporal transcriptomic divergence across human and macaque brain development. Science 362, eaat8077 (2018). [PubMed: 30545855]
16. Pollen AA et al. Establishing cerebral organoids as models of human-specific brain evolution. Cell 176, 743–756 (2019). [PubMed: 30735633]
17. Kanton S et al. Organoid single-cell genomic atlas uncovers human-specific features of brain development. Nature 574, 418–422 (2019). [PubMed: 31619793]
18. Johnson MB et al. Functional and evolutionary insights into human brain development through global transcriptome analysis. Neuron 62, 494–509 (2009). [PubMed: 19477152]
19. Pletikos M et al. Temporal specification and bilaterality of human neocortical topographic gene expression. Neuron 81, 321–332 (2014). [PubMed: 24373884]
20. Li M et al. Integrative functional genomic analysis of human brain development and neuropsychiatric risks. Science 362, eaat7615 (2018). [PubMed: 30545854]
21. Urade Y et al. Precerebellin is a cerebellum-specific protein with similarity to the globular domain of complement C1q B chain. Proc. Natl. Acad. Sci. U. S. A 88, 1069–1073 (1991). [PubMed: 1704129]
22. Hirai H et al. Cbln1 is essential for synaptic integrity and plasticity in the cerebellum. Nat. Neurosci 8, 1534–1541 (2005). [PubMed: 16234806]

23. Uemura T et al. Trans-synaptic interaction of GluRdelta2 and Neurexin through Cbln1 mediates synapse formation in the cerebellum. Cell 141, 1068–1079 (2010). [PubMed: 20537373]
24. Matsuda K et al. Cbln1 is a ligand for an orphan glutamate receptor delta2, a bidirectional synapse organizer. Science 328, 363–368 (2010). [PubMed: 20395510]
25. Yasumura M et al. Glutamate receptor delta1 induces preferentially inhibitory presynaptic differentiation of cortical neurons by interacting with neurexins through cerebellin precursor protein subtypes. J. Neurochem 121, 705–716 (2012). [PubMed: 22191730]
26. Wei P et al. The Cbln family of proteins interact with multiple signaling pathways. J. Neurochem 121, 717–729 (2012). [PubMed: 22220752]
27. Seigneur E & Sudhof TC Genetic ablation of all cerebellins reveals synapse organizer functions in multiple regions throughout the brain. J. Neurosci 38, 4774–4790 (2018). [PubMed: 29691328]
28. Elston GN Pyramidal cells of the frontal lobe: all the more spinous to think with. J. Neurosci 20, RC95 (2000). [PubMed: 10974092]
29. Jacobs B et al. Regional dendritic and spine variation in human cerebral cortex: a quantitative golgi study. Cereb. Cortex 11, 558–571 (2001). [PubMed: 11375917]
30. Bianchi S et al. Synaptogenesis and development of pyramidal neuron dendritic morphology in the chimpanzee neocortex resembles humans. Proc. Natl. Acad. Sci. U. S. A 110, 10395–10401 (2013). [PubMed: 23754422]
31. Molliver ME et al. The development of synapses in cerebral cortex of the human fetus. Brain Res. 50, 403–407 (1973). [PubMed: 4705508]
32. Voigt T et al. Synaptophysin immunohistochemistry reveals inside-out pattern of early synaptogenesis in ferret cerebral cortex. J. Comp. Neurol 330, 48–64 (1993). [PubMed: 8468403]
33. Rakic P et al. Concurrent overproduction of synapses in diverse regions of the primate cerebral cortex. Science 232, 232–235 (1986). [PubMed: 3952506]
34. Shibata M et al. Regulation of prefrontal patterning, connectivity and synaptogenesis by retinoic acid. Accompanying paper.
35. Kang HJ et al. Spatiotemporal transcriptome of the human brain. Nature 478, 483–489 (2011). [PubMed: 22031440]
36. Lambert N et al. Genes expressed in specific areas of the human fetal cerebral cortex display distinct patterns of evolution. PLoS One 6, e17753 (2011). [PubMed: 21445258]
37. Miller JA et al. Transcriptional landscape of the prenatal human brain. Nature 508, 199–206 (2014). [PubMed: 24695229]
38. ENCODE Project Consortium. et al. An integrated encyclopedia of DNA elements in the human genome. Nature 489, 57–74 (2012). [PubMed: 22955616]
39. Chiang MY et al. An essential role for retinoid receptors RARbeta and RXRgamma in long-term potentiation and depression. Neuron 21, 1353–1361 (1998). [PubMed: 9883728]
40. Krezel W et al. Impaired locomotion and dopamine signaling in retinoid receptor mutant mice. Science 279, 863–867 (1998). [PubMed: 9452386]
41. Kwan KY et al. SOX5 postmitotically regulates migration, postmigratory differentiation, and projections of subplate and deep-layer neocortical neurons. Proc. Natl. Acad. Sci. U. S. A 105, 16021–16026 (2008). [PubMed: 18840685]
42. Shim S et al. Cis-regulatory control of corticospinal system development and evolution. Nature 486, 74–79 (2012). [PubMed: 22678282]
43. Clarke RA & Eapen V Balance within the neurexin trans-synaptic connexus stabilizes behavioral control. Front. Hum. Neurosci 8, 52 (2014). [PubMed: 24578685]
44. State MW & Sestan N The emerging biology of autism spectrum disorders. Science 337, 1301–1303 (2012). [PubMed: 22984058]
45. Sudhof TC Synaptic neurexin complexes: A molecular code for the logic of neural circuits. Cell 171, 745–769 (2017). [PubMed: 29100073]
46. Willsey AJ et al. Coexpression networks implicate human midfetal deep cortical projection neurons in the pathogenesis of autism. Cell 155, 997–1007 (2013). [PubMed: 24267886]
47. Gulsuner S et al. Spatial and temporal mapping of de novo mutations in schizophrenia to a fetal prefrontal cortical network. Cell 154, 518–529 (2013). [PubMed: 23911319]

48. Lewis DA & Mirnics K Transcriptome alterations in schizophrenia: disturbing the functional architecture of the dorsolateral prefrontal cortex. Prog. Brain Res 158, 141–152 (2006). [PubMed: 17027695]

Extended References

49. Dy P, Han Y & Lefebvre V Generation of mice harboring a Sox5 conditional null allele. Genesis 46, 294–299 (2008). [PubMed: 18543318]

50. Mathelier A et al. JASPAR 2016: a major expansion and update of the open-access database of transcription factor binding profiles. Nucleic Acids Res. 44, D110–D115 (2016). [PubMed: 26531826]

51. Khan A et al. JASPAR 2018: Update of the open-access database of transcription factor binding profiles and its web framework. Nucleic Acids Res 46, D260–D266 (2018). [PubMed: 29140473]

52. Shim S et al. Regulation of EphA8 gene expression by TALE homeobox transcription factors during development of the mesencephalon. Mol. Cell Biol 27, 1614–1630 (2007). [PubMed: 17178831]

53. Wang H et al. One-step generation of mice carrying mutations in multiple genes by CRISPR/Cas-mediated genome engineering. Cell 153, 910–918 (2013). [PubMed: 23643243]

54. Liu P et al. A highly efficient recombineering-based method for generating conditional knockout mutations. Genome Res 13, 476–484 (2003). [PubMed: 12618378]

55. Cong L et al. Multiplex genome engineering using CRISPR/Cas systems. Science 339, 819–823 (2013). [PubMed: 23287718]

56. Wilkinson DG & Nieto MA Detection of messenger RNA by in situ hybridization to tissue sections and whole mounts. Methods Enzymol. 225, 361–373 (1993). [PubMed: 8231863]

57. Hunt CA et al. PSD-95 is associated with the postsynaptic density and not with the presynaptic membrane at forebrain synapses. J. Neurosci 16, 1380–1388 (1996). [PubMed: 8778289]

58. Essrich C et al. Postsynaptic clustering of major GABAA receptor subtypes requires the gamma 2 subunit and gephyrin. Nat. Neurosci 1, 563–571 (1998). [PubMed: 10196563]

59. Ippolito DM & Eroglu C Quantifying synapses: an immunocytochemistry-based assay to quantify synapse number. J. Vis. Exp 45, 2270 (2010).

60. Fiala JC Reconstruct: A free editor for serial section microscopy. J. Microsc 218, 52–61 (2005). [PubMed: 15817063]

61. Risher WC et al. . Rapid golgi analysis method for efficient and unbiased classification of dendritic spines. PLoS One 9, (2014)

62. Kaur N et al. Neural stem cells direct axon guidance via their radial fiber scaffold. Neuron 107, 1197–1211 (2020). [PubMed: 32707082]

63. Meijering E et al. Design and validation of a tool for neurite tracing and analysis in fluorescence microscopy images. Cytom. Part A 58, 167–176 (2004).

64. Hinrichs AS et al. The UCSC Genome Browser database: update 2006. Nucleic Acids Res. 34, D590–598 (2006). [PubMed: 16381938]

65. Robinson JT et al. Integrative genomics viewer. Nat. Biotechnol 29, 24–26 (2011). [PubMed: 21221095]

66. Kent WJ et al. The human genome browser at UCSC. Genome Res. 12, 996–1006 (2002). [PubMed: 12045153]

67. Rosenbloom KR et al. ENCODE data in the UCSC Genome Browser: year 5 update. Nucleic Acids Res. 41, D56–63 (2013). [PubMed: 23193274]

68. Shibata M et al. MicroRNA-9 regulates neurogenesis in mouse telencephalon by targeting multiple transcription factors. J. Neurosci 31, 3407–3422 (2011). [PubMed: 21368052]

69. Morozov YM, Ayoub AE & Rakic P Translocation of synaptically connected interneurons across the dentate gyrus of the early postnatal rat hippocampus. J. Neurosci 26, 5017–5027 (2006). [PubMed: 16687493]

70. Morozov YM, Mackie K & Rakic P Cannabinoid type 1 receptor is undetectable in rodent and primate cerebral neural stem cells but participates in radial neuronal migration. Int. J. Mol. Sci 21, 1–19 (2020).

71. Thompson CL et al. A high-resolution spatiotemporal atlas of gene expression of the developing mouse brain. Neuron 83, 309–323 (2014). [PubMed: 24952961]

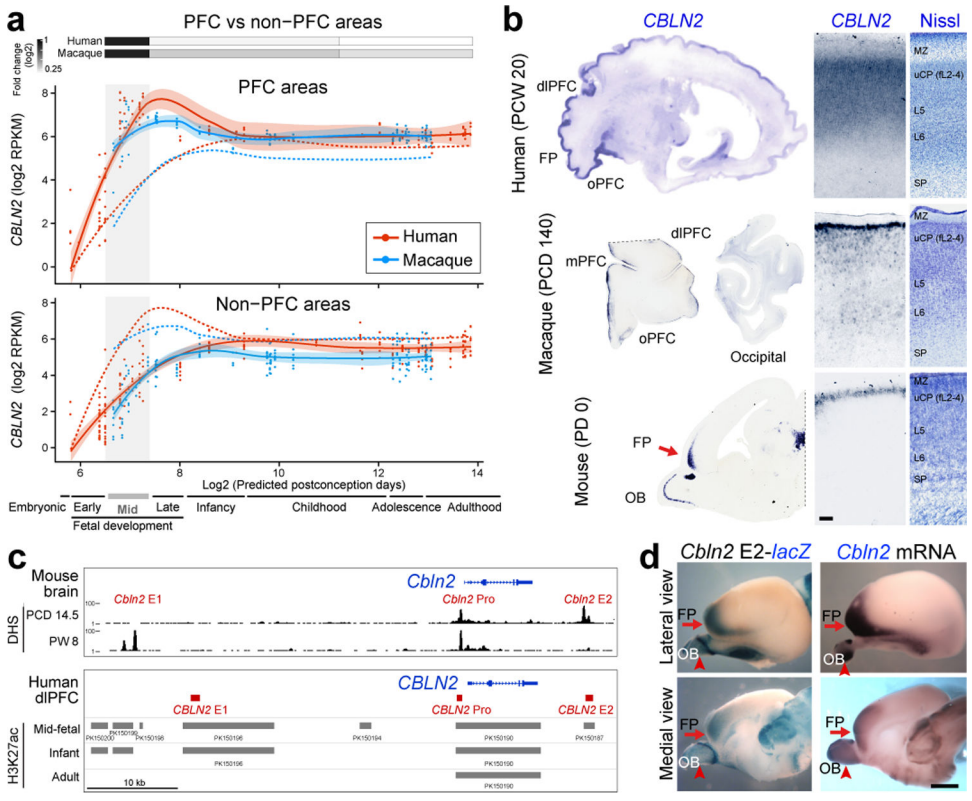

Fig. 1 |. Phylogenetic, transcriptomic, and regulatory characterization of developmental PFC upregulation of *CBLN2*.

a, *CBLN2* spatiotemporal expression in human (red lines) and macaque (blue lines) PFC (solid lines) and non-PFC (dotted lines) areas. Quantification of fold change between PFC and non-PFC expression for periods 4–6 (gray box), 7–10 and 11–14 (two-tailed Mann-Whitney test or two-tailed unpaired t-test $P < 1e\text{-}4$ for all comparisons) shown above plots. For all of the plots, the shading around the lines represents the 95% confidence interval. Developmental periods designed by Kang et al.[35] are shown below. **b,** *CBLN2 in situ* hybridization on sagittal sections of midfetal human and a neonatal mouse and coronal sections of midfetal macaque prefrontal and occipital lobes. Right panels show laminar *CBLN2* expression pattern in PFC and Nissl stain of adjacent section. Human *CBLN2* image is from humanbraintranscriptome.org [18,19,37]. Experiments were repeated three times for Macaque brain sections and more than five times for mouse brain sections. FP, frontal pole; MZ, marginal zone; SP, subplate; uCP, upper cortical plate. Scale bars, 500 μm. **c,** DNase 1 hypersensitive sites (DHS) in mouse brain at PCD 14.5 and PW 8 within 50 kb either upstream and downstream of *Cbln2* gene. H3K27ac ChIP-seq data from human dlPFC/DFC at mid-fetal age, infancy, and adulthood (bottom panel). Putative *cis*-regulatory elements were designated as *CBLN2* E1, E2, and Pro. **d** β-Galactosidase activity in transgenic mouse brain carrying mouse *Cbln2* E2 conjugated with *lacZ* reporter at PCD 17. Endogenous *Cbln2* expression in age-matched brains by *in situ* hybridization is shown for comparison. Arrows depict FP; arrowheads, olfactory bulb (OB). Scale bars, 1mm. Experiments were repeated for three brains and two replicates are shown in Extended Data Fig. 3c.

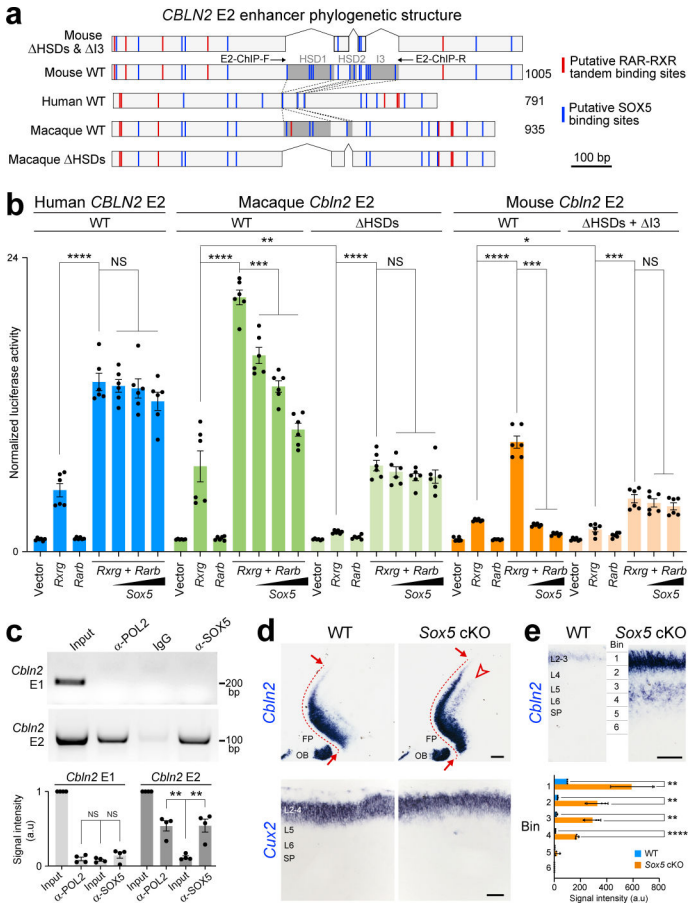

Fig. 2 |. SOX5 represses *CBLN2* through Hominini-specific regulatory deletions.

a, Schematics of *Cbln2* E2 constructs used for luciferase assays. Shaded dark grey areas in indicate HSD1-2 and I3 (mouse) and HSD1-2 (macaque). All HSDs and I3 are deleted from mouse *Cbln2* E2 in ΔHSDs & ΔI3, and all HSDs are deleted from macaque *Cbln2* E2 in macaque ΔHSDs. Red and blue lines indicate putative RAR-RXR tandem and SOX5 binding sites, respectively. E2-ChIP-F and R represent ChIP-PCR primers (c) (Table S1). **b,** *Cbln2* E2 luciferase assay in Neuro-2a cells with mouse *Rxrg* and *Rarb* and increasing concentrations of *Sox5*. Two-tailed Student's t-test; *P = 0.01; **P = 0. 001; ***P = 4e-4 (Macaque), 4e-4 (mouse), 7e-5 (mouse ΔHSDs + ΔI3); ****P < 1e-5, NS, not significant. Error bars: S.E.M.; N = 6 per condition. **c,** ChIP-PCR assays in PD 0 mouse neocortex using anti-RNA polymerase II (anti-POL2), IgG, and anti-SOX5 and *Cbln2* E1 and E2 primers and quantifications of signal intensity below. Two-tailed Student's t-test; **P = 0.001, 0.003; Error bars: S.E.M.; N = 4 per condition. **d,** *Cbln2* expression in PD 0 *Sox5* cKO compared to *Sox5* +/+; *Emx1-Cre* (WT) cortex. N = 3 per genotype. Arrows indicate posterior spread of *Cbln2* expression and arrowheads indicate ectopic deep layer expression. FP, frontal pole; OB, olfactory bulb. Scale bars, 200 μm (top); 100 μm (bottom). **e,** Quantification of cortical *Cbln2* signal intensity in six bins spanning from pia to ventricular zone (N = 3). Two-tailed Student's t-test; ****P = 2e-5 (Bin4); **P = 3e-3 (Bin1), 2e-3 (Bin2), 1e-3 (Bin3). Scale bar, 100 μm.

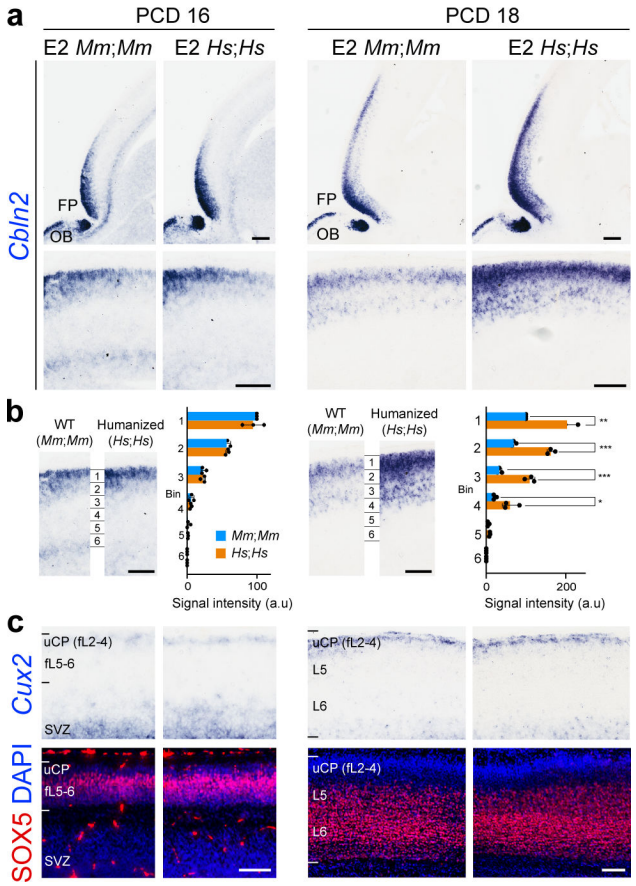

Fig. 3 |. *In situ* genetic humanization of the mouse *Cbln2* enhancer drives upregulation and ectopic laminar *Cbln2* expression in the neonatal frontal cortex.

a, *Cbln2* expression in the humanized *Cbln2* E2 knock-in mouse (h*Cbln2* E2, *Hs;Hs*) brain at PCD 16 and 18 compared to WT mouse (*Cbln2* E2, *Mm;Mm*) with higher magnification panels below. FP, frontal pole; OB, olfactory bulb. Scale bars, 200 μm (top); 100 μm (bottom). Experiments were repeated for three brains and two replicates are shown in Extended Data Fig. 8. **b,** Neocortex was divided into six equal bins spanning from pia to ventricular zone, and *Cbln2* signal intensity was quantified for each bin and compared between WT and h*Cbln2* E2 (*Hs;Hs*). Two-tailed Student's t-test; *P = 0.02 (PCD 18), 0.02, 0.04 (PD 1), **P = 1e-3 (PCD18), 1e-3, 3e-3, 3e-3 (PD 1), ***P = 1e-4, 2e-4 (PCD 18); N = 3 per genotype. Scale bars, 100 μm. **c,** Expression of the upper layer marker, *Cux2,* and SOX5 in adjacent tissue sections were detected by *in situ* hybridization and immunostaining, respectively. Scale bars, 100 μm. N = 3.

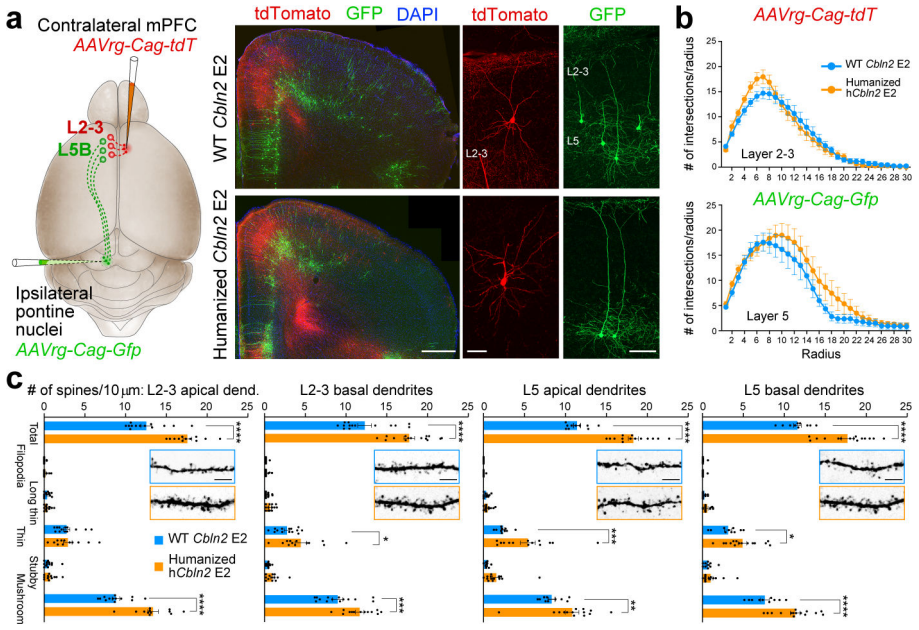

Fig. 4 |. Increased density of dendritic spines in the mPFC of humanized *CBLN2* E2 mice.

a, Retrogradely labeled callosal L2-3 (red; *AAVrg-Cag-tdT*) and subcerebral L5B (green; *AAVrg-Cag-Gfp*) PD 60 pyramidal neurons. Scale bars, 500 µm (left); 20 µm (right). Three brains from each genotype were injected. **b,** Sholl analysis of retrogradely labelled L2-3 (top) and L5 (below). Two-way ANOVA with Sidak's multiple comparison method. Error bars: S.E.M.; N = 13 (WT *Cbln2* E2), and 15 (h*Cbln2* E2) L2-3; N = 11 (WT *Cbln2* E2), and 15 (h*Cbln2* E2) L5 (N = 3 brains per genotype). **c,** Quantification of dendritic spines. Two-way ANOVA with Sidak's multiple comparison method; *P = 0.03 (L2-3 basal dendrites), 0.03 (L5 basal dendrites); **P = 5e-3, ***P = 4e-4 (L2-3 basal dendrites), 4e-4 (L5 apical dendrites); ****P < 5e-5; Error bars: S.E.M.; N = 13 (WT *Cbln2* E2), and 12 (h*Cbln2* E2) L2-3 apical dendrites; N = 14 (WT *Cbln2* E2) and N = 15 (h*Cbln2* E2*)* L2-3 basal dendrites; N = 10 (WT *Cbln2* E2), and 14 (h*Cbln2* E2) L5 apical dendrites; N = 10 (WT *Cbln2* E2) and N = 15 (h*Cbln2* E2*)* L5 basal dendrites (N = 3). Scale bar, 10 µm.